Modern Chemistry
2024, Vol. 12, No. 1, pp. 6-27
https://doi.org/10.11648/j.mc.20241201.12

Research Article

Synthesis and Performance of a New and Simple Schiff Base Structure for Corrosion Inhibition of C38 steel in 1 M HCl Solution: Experimental Studies and DFT Investigation

Armel Megha Nouteza[1], Martin Pengou[1, 2, 3 *], Joliot Perrin Mbiamy Ngamy[1], Pengkun Hou[4], Jean Jacques Kouadjo Tchekwagep[5], Charles P éguy Nanseu-Njiki[1], Emmanuel Ngameni[1]

[1]Department of Inorganic Chemistry, Faculty of Sciences, University of Yaounde 1, Yaounde, Cameroon

[2]Department of Chemistry, Faculty of Sciences, University of Maroua, Maroua, Cameroon

[3]Department of Mineral Engineering, School of Chemical Engineering and Mineral Industries, University of Ngaoundere, Ngaoundere, Cameroon

[4]School of Materials Science and Engineering, University of Jinan, Jinan, China

[5]Shandong Provincial Key Laboratory of Preparation and Measurement of Building Materials, University of Jinan, Jinan, China

Abstract

In order to investigate the corrosion of carbon steel (C38) in acidic media, experimental studies (weight loss measurements, electrochemical methods, thermodynamic adsorption isotherms and field emission scanning electron microscopy coupled with energy dispersive X-ray) and computational approach were adopted to study the newly synthesized and simple Schiff base structure, namely 4-((phenylimino)methyl) phenol (PIMP) as a corrosion inhibitor for C38 steel in 1M HCl. Characterization techniques (Fourier Transform Infrared spectroscopy, mass spectrometry, proton nuclear magnetic resonance) showed that PIMP was successfully synthesized with a yield of 63%. Experimental methods (weight loss, open circuit potential (OCP), electrochemical impedance spectroscopy (EIS), potentiodynamic polarization (PDP)) showed that PIMP is a mixed-type inhibitor with an inhibition percentage of 91.1% under optimal conditions (7.5 mM PIMP at 30 ℃). These experimental results were supported by surface analysis (Field Emission Scanning Electron Microscopy (FESEM) coupled with Energy Dispersive X-Ray (EDX)), where PIMP molecules are adsorbed on the steel surface and form a protective barrier against aggressive ions, thereby limiting steel oxidation. The adsorption of PIMP on the carbon steel surface followed the Langmuir adsorption isotherm along with a mixture of physical and chemical adsorption, forming a complete and dense protective film on the C38 steel surface. Theoretical results using density functional theory (DFT) calculations showed that PIMP contains highly reactive centers and confirmed the experimental results obtained.

Keywords

Corrosion Inhibition, Schiff Base, Carbon Steel, DFT

*Corresponding author: mapesu@yahoo.fr (Martin Pengou)

Received: 20 March 2024; **Accepted:** 12 April 2024; **Published:** 29 April 2024

1. Introduction

Carbon steel is one of the most common and least expensive materials used in almost all industrial processes. This is due to its many properties, such as machinability, ductility, high melting point, and good thermal and electrical conductivity. However, one of the main problems in industrial development is the degradation of steel due to a corrosion process. Corrosion refers to all phenomena in which a metal or metal alloy tends to oxidize under the influence of gaseous or liquid reactants. This irreversible process causes heavy economic losses in most industries (oil, food, water treatment, etc.), resulting in production stoppages, replacement of corroded parts, accidents and pollution risks. [1-3] The losses caused by corrosion could be minimized by a better understanding of this phenomenon and a better application of safe and less costly techniques.

To date, many techniques have been developed to control and prevent corrosion in an aggressive environment (acidic environments, neutral or alkaline chloride media, etc.), such as the application of coatings, sacrificial anode protection, galvanizing, or the use of corrosion inhibitors. [4-7] However, corrosion inhibitors could be used to protect steel. This does not require any significant maintenance of the technical equipment requiring this corrosion protection.

A corrosion inhibitor is a chemical compound that, when added at low concentrations to a corrosive environment, slows or stops the corrosion process of the metal. Many organic and inorganic molecules have been successfully used as corrosion inhibitors for steel; however, due to environmental constraints due to their high toxicity and ecological aspects, inorganic inhibitors are gradually being banned and organic molecules are increasingly being used. [8, 9] Thus, one of the most environmentally friendly, cost-effective and practical approaches is the use of organic inhibitors, given the large amount of work carried out on this subject. [6, 10, 11] Organic inhibitors have heteroatoms (nitrogen, oxygen, sulfur and phosphorus) and pi-conjugated systems responsible for their corrosion inhibition mechanism. In fact, they act by an adsorption mechanism on the surface of metals and alloys through these electron-rich sites, forming a protective barrier against aggressive agents present in the solution and preventing oxidation of metals and alloys [12-16].

Among the organic inhibitors (plant extracts, quinoxaline derivatives, epoxy resin, Schiff bases, etc.), Schiff bases have been extensively studied as acid corrosion inhibitors for carbon steel. [Schiff bases are organic compounds containing an imine (>C=N-) group with the general formula R3R2C=NR1, where R1 is H; R1, R2 and R3 can be aryl or alkyl groups. They are also known as imines, azomethines or anils. [18] They are formed by the reaction of a primary amine with an aldehyde or ketone. Schiff bases play an important role as potent antimicrobial agents. [19, 20] They are also used as polydentate ligands for the synthesis of metal complexes. [21, 22] To date, several Schiff bases have been reported as corrosion inhibitors of metals and alloys in acidic environments. [14, 15, 23-27] The increasing number of Schiff's bases used as corrosion inhibitors is mainly due to their low toxicity and affordable synthesis reagents. [10] Numerous publications on organic corrosion inhibitors have demonstrated that Schiff's bases have much higher inhibition efficiencies than the aldehydes, ketones, and amines from which they are derived. [27-29] In addition, the literature indicates that the synthesis of polydentate Schiff's bases, which have many heteroatoms and pi-conjugated systems, is much more complex and requires synthetic processes that are not easily implemented. [30-32] However, these polydentate Schiff bases (large molecules) do not necessarily guarantee excellent corrosion inhibition of carbon steels in acid medium. [33-35] The synthesis of a simple Schiff base (a small molecule), which is easy to obtain and has structural elements that allow it to be adsorbed on the steel surface in an acidic medium, would be very interesting for the investigations related to the corrosion inhibition of carbon steels using Schiff bases. Indeed, one of the major issues in the field of corrosion inhibition today is the use of effective, inexpensive and readily available inhibitors, given the large financial losses already caused by corrosion itself [7, 15].

Therefore, the aim of this work is to investigate the inhibitory activity of a new and simple monodentate Schiff base on the corrosion of C38 steel in 1 M hydrochloric acid medium. The imine, namely 4-((phenylimino)methyl)phenol (PIMP), was obtained from the condensation reaction between 4-hydroxybenzaldehyde and phenylamine. Characterization of the synthesized molecules was performed by Fourier transform infrared spectroscopy (FTIR), mass spectroscopy (MS), and proton nuclear magnetic resonance (^{1}H NMR). The corrosion rate and inhibitory activity of PIMP were evaluated by weight loss measurements and electrochemical measurements (open circuit potential, electrochemical impedance spectroscopy, and potentiodynamic polarization). The reaction surface of C38 steel was characterized by field emission scanning electron microscopy (FESEM) coupled with energy dispersive X-ray (EDX) spectroscopy. In addition to the experimental studies, computational studies using Density Functional Theory (DFT) were also carried out to obtain a theoretical estimate of the inhibitory performance of the PIMP molecules and to provide the elements needed to better understand the corrosion inhibition mechanism of the steel.

2. Materials and Methods

2.1. Metal Samples

The corrosion studies were carried out on a cylindrical sample of C38 steel 1 cm in diameter, supplied by Tacinas

Company, France. Its chemical composition is as follows (% by mass): 0.360 C; 0.230 Si; 0.680 Mn; 0.016S; 0.077 Cr; 0.011 Ti; 0.059 Ni; 0.009 Co; 0.160 Cu and Fe (remaining). For corrosion measurements, the side surface of the C38 steel rod was coated with polytetrafluoroethylene (PTFE), leaving its free circular base area of 0.785 cm^2. In order to obtain reproducible electrochemical measurements, this reaction surface (working electrode) was abraded beforehand using silicon carbide abrasive papers of different grain sizes (500, 1000, 1200 and 2400). Starting from the most abrasive to the least abrasive then this surface was rinsed with deionized water and dried with ethanol.

2.2. Working Solution

The corrosive solution was prepared from a commercial solution of 37% hydrochloric acid (Scharlau) and deionized water. In order to be able to develop an inhibitor for a strongly acidic medium and to be able to compare the results obtained with those of the literature, the investigations were carried out in 1M HCl medium. All electrochemical measurements unless otherwise stated were performed in an electrochemical cell thermostated at 30 ℃.

2.3. Synthesis and Characterization of 4-((phenylimino)methyl) phenol (PIMP)

2.3.1. Synthesis Equation of PIMP

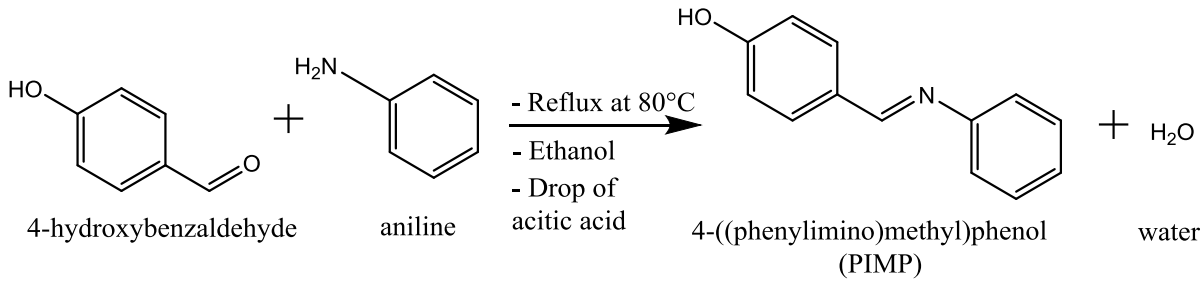

Scheme 1. *Synthesis equation of PIMP.*

2.3.2. Synthesis Procedures

1) Introduce 4-hydroxybenzaldehyde (Sigma-Aldrich, 98%, 6.18 g, 50 mmol) into a 100 mL flask, then add ethanol (98 °, 25 mL) with a few drops of acetic acid (Scharlau) and stir at 80 ℃.
2) Once the compound has dissolved, add aniline (Prolabo, 100%, 4.5 mL, 50 mmol) dissolved in 25 mL of ethanol, and bring to reflux.
3) After 3 hours, the solution is removed from reflux and left at ambient temperature and 30 minutes later, the formation of a precipitate is observed.
4) Place the solution in an ice bath for about 10 min.
5) Remove the solution from the ice bath and allow to return to room temperature then filter.
6) The recrystallization was carried out in ethanol/water ratio (1:1).

2.3.3. Solubility Tests

PIMP molecule is soluble in polar solvents such as dimethylformamide, dimethyl sulfoxide, methane-dichloride, 2-propanone and ethanol. It is noted that PIMP molecule dissolves in the aggressive solution after agitation.

2.3.4. Characterization of PIMP

The chemical characterization was carried out in order to elucidate the chemical structure of the synthesized compound via different techniques: Fourier transform infrared spectrum (IR-TF) on a Bruker Alpha FTIR-8300 spectrometer, mass spectrum on the MALDI/TOF BRUKER spectrometer and nuclear magnetic resonance spectrum (NMR ^1H) on a Bruker Spectro spin instrument at 300mMHz Ultra Shield magnets.

2.4. Gravimetric Measurement

Weight loss study was performed using cubic samples of 1 cm in length with the same carbon steel composition of the working electrode, were abraded successively with different grades of silicon carbide abrasive papers (500; 1000; 1200 and 2400), washed with deionized water and dried with ethanol. After being weighed using a ± 0.0001 g precision balance. The surfaces of the sample were coated with polytetrafluoroethylene (PTFE), leaving its free square base area of 1 cm^2. The specimens were immersed in 1M HCl with and without various concentrations of the studied compounds in aerated condition at room temperature. After a 24 hours immersion, the samples were taken out, thoroughly rinsed with deionized water, dried and further weighed accurately.

The corrosion rate C_{RW} (mg.cm^{-2}.h^{-1}) was calculated using equation 1:

$$C_{RW} = \frac{W}{S.t} \quad (1)$$

Where, W is the weight loss of carbon steel sample, S is the total area of carbon steel sample and t is immersion time (24 hours). The inhibition efficiency E_W (%) was calculated using equation 2:

$$E_W(\%) = \left(\frac{C^{\circ}_{RW} - C_{RW}}{C^{\circ}_{RW}}\right) \times 100 \quad (2)$$

Where C°_{RW} and C_{RW} are uninhibited and inhibited corrosion rates, respectively.

The precision of the corrosion rate is calculated by using three different measurements. Standard deviation of the corrosion rate is also calculated.

2.5. Electrochemical Measurements

The electrochemical measurements were carried out in a thermostatically controlled electrochemical cell containing three electrodes. The working electrode is a cylindrical rod of 0.785 cm^2 in surface of C38 steel, Auxiliary electrode is of platinum with 0.092 cm^2 in surface and the reference electrode is a saturated calomel electrode (SCE). These three electrodes are connected to an Autolab PGSTAT Potentiostat / Galvanostat which has an impedance module and is controlled by Frequency Response Analyzer (FRA) for electrochemical impedance spectroscopy (EIS) measurements and General Purpose Electrochemical Software (GPES) softwares for open circuit potential (OCP), and potentiodynamic polarization (PDP) measurements. Before each recording of the OCP, EIS and PDP curves, the reactional surface of C38 steel is first immersed in an aggressive solution for 1 hour without and with different concentrations of inhibitor in order to reach a quasi-stationary time necessary for the other electrochemical measurements. The polarization curves are recorded at $\pm$300 mV/SCE of the corrosion potential with a scanning speed of 1 mV/s. The electrochemical parameters such as the corrosion current (I_{corr}), the anodic and cathodic Tafel slopes (b_a and b_c) and the polarization resistance (R_p) are obtained by fitting the experimental curves using the EC-Lab V11.2.1 software.

The inhibition percentage calculated from I_{corr} and R_p are given by equations 3-4:

$$E_{Icorr} = (I'_{corr} - I_{corr}) \times 100/I'_{corr} \quad (3)$$

$$E_{Rp} = (Rp - Rp') \times 100/Rp \quad (4)$$

Where *Icorr'* and *Rp'* are respectively the corrosion current and the polarization resistance in the absence of inhibitor; *Icorr* and *Rp* are respectively the corrosion current and the polarization resistance in the presence of inhibitor.

The EIS curves are recorded at the corrosion potential with an amplitude of 10mV, in a frequency range of 10^4 Hz to 10^{-2} Hz. The experimental data are also processed using the EC-Lab V11.2.1 software.

The inhibitory efficacy calculated from the EIS data is given by equation 5:

$$\eta_{Rct} = (Rct - Rct') \times 100/Rct \quad (5)$$

Where *Rct'* is the charge transfer resistance in the absence of inhibitor and *Rct* that in the presence of inhibitor.

Each manipulation is repeated three times in order to ensure the reproducibility of the results.

2.6. The Field Emission Scanning Electron Microscopy (FESEM) and Energy Dispersive X-ray (EDX) Analysis

FESEM/EDX analyzes were used to study the morphology and the elemental composition of the C38 steel surface after 5 hours of immersion in 1M HCl solution in the absence and in the presence of the optimal concentration of inhibitor. These analyzes were carried out using HYROX SH-3000 and EDX-BRUKER devices.

2.7. Quantum Chemical Analysis

2.7.1. Global Quantum Chemical Reactivity

The electronic quantum chemistry applying the density functional theory (DFT) method was adopted to computationally study the electronic-structure of PIMP and his protonated form PIMPH$^+$ to arrive at a better comprehension of the link between the structure of this molecule and his inhibitory efficiency utilizing Gaussian 09W 9.5 Revision D.01 software coupled with GaussView 5.0.8 software. The quantum chemical descriptors were computed using DFT method at the Becke-3-parameter-Lee–Yang–Parr (B3LYP) level on the 6-31G (d, p) basis in the aqueous phase. [2] These descriptors were computed four times and the mean value and the standard deviation were obtained and presented.

2.7.2. Fukui Indices and Dual Fukui Descriptors

The reactivity of the local sites that accountable for interactions with Fe-surface were investigated by means of condensed Fukui indices [5], local softness (σ_k^{α}), and local electrophilicity (ω_k^{α}) according equations 6-8.

$$f_k^+ = q_k(N+1) - q_k(N) \; (for\ nucleophilic\ attacks) \quad (6)$$

$$f_k^- = q_k(N) - q_k(N-1) \; (for\ electrophilic\ attacks) \quad (7)$$

$$\sigma_k^{\alpha} = Sf_k^{\alpha} \; and \; \omega_k^{\alpha} = \omega f_k^{\alpha} \quad (8)$$

where $q_k(N)$, $q_k(N+1)$ and $q_k(N-1)$ are the charges

values of atom k for neutral, cation and anion species, respectively. Also, the $\alpha = +, -$ and 0 corresponds to local softness quantities describing nucleophilic, electrophilic, and radical attacks, respectively. More precisely, the dual Fukui descriptor or the second order Fukui functions (f_k^2), the associated dual local softness ($\Delta\sigma_k$) and the dual local philicity ($\Delta\omega_k$) are used to give a simple and instinctive way to chemical reactivity in a local sense. These dual descriptors are defined as follows equation 9 [5]:

$$f_k^2 = f_k^+ - f_k^-, \Delta\sigma_k = \sigma_k^+ - \sigma_k^- \; and \; \Delta\omega_k = \omega_k^+ - \omega_k^- \quad (9)$$

3. Results and Discussion

3.1. Synthesis and Characterization of PIMP

4-((phenylimino)methyl) phenol (PIMP) was obtained following the condensation reaction between phenylamine and 4-hydroxybenzaldehyde according to Scheme 2:

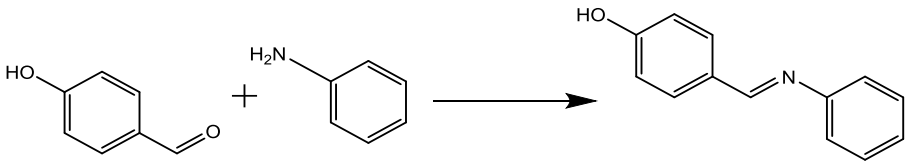

Scheme 2. *Synthesis equation of PIMP.*

PIMP inhibitor is soluble in polar solvents such as dimethylformamide, dimethyl sulfoxide, methane-dichloride, 2-propanone, and ethanol. The Fourier transform IR spectrum of PIMP reveals the appearance of a new absorption band at 1583 cm^{-1}, attributable to the azomethine group. The disappearance of the absorption bands of the carbonyl and amine functional groups is also noted. Analysis of the chemical ionization mass spectrum shows that the peak of the molecular ion has an m/z ratio equal to 197.973 ≈ 198 g/mol. Knowing the expected structure of the molecule whose molar mass is 197 g/mol, we can affirm that the molecular ion is [M+H]+, thereby confirming the effective synthesis and purity of PIMP. Figure 1 shows the nuclear Magnetic resonance (NMR) protons of PIMP. The NMR proton spectrum of PIMP showed that the azomethine proton (H4) appears at 8.44 ppm.

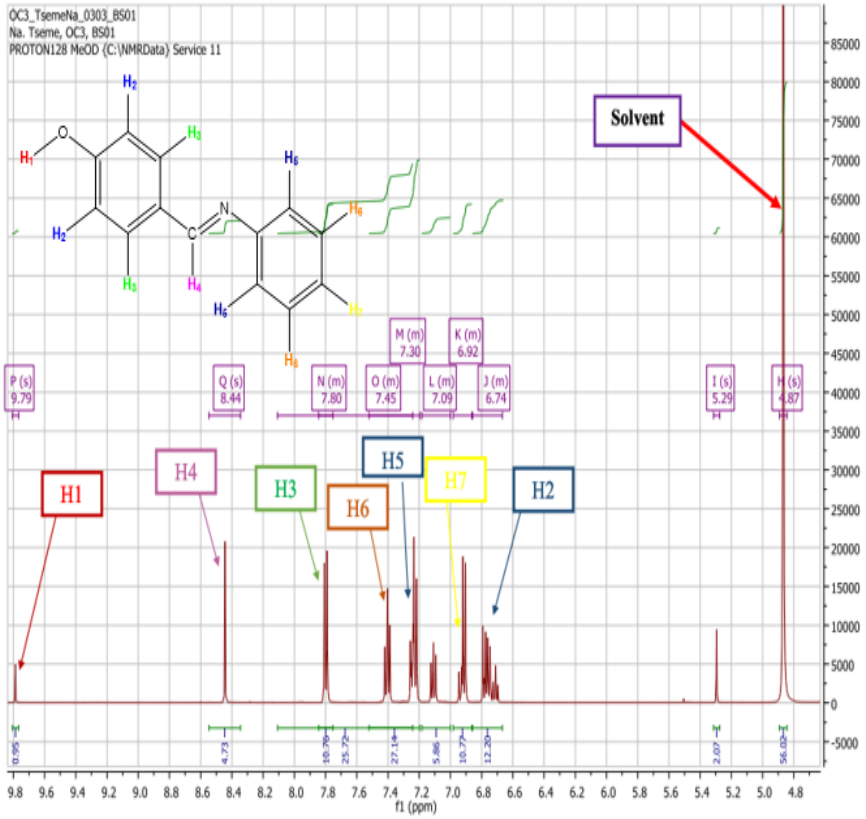

Figure 1. *Elucidation 1H NMR spectrum of PIMP synthetized.*

Therefore, all characterization techniques show that Schiff's base molecule (4-((phenylimino)methyl)phenol) has been successfully synthesized.

3.2. Gravimetric Measurement

Table 1 presents the values of the corrosion rate and inhibitory efficacy calculated by the gravimetric method at various concentrations of PIMP in 1M hydrochloric acid at room temperature 30±1 ℃, after 24 h of immersion. Furthermore, accuracy is essential to determine whether the mass loss measurement is properly. It can be seen that the corrosion rate (CRW) decreased when the concentration of the inhibitor increased, and that the inhibition percentage (EW) increased up to maximum value of 79.9% at 10mM of PIMP. This increase is probably due to the adsorption of the inhibitor, which forms a protective layer on the surface of the steel and prevents the latter from dissolving.

Table 1. *Corrosion parameters of the mass loss of C38 steel after 24 hours of immersion in 1 M HCl medium at different concentrations of PIMP at room temperature.*

Conc (mM)	C_{RW} (mg.cm^{-2}.h^{-1})			C_{RW} Mean	Standard Deviation	Precision Result	E_W (%)
	Test 1	Test 2	Test 3				
Blank	0.72	0.60	0.68	0.66	0.05	0.66 ± 0.05	/
1	0.32	0.28	0.29	0.30	0.02	0.30 ± 0.02	55.4
2.5	0.19	0.18	0.20	0.19	0.01	0.19 ± 0.01	71.8
5	0.17	0.15	0.18	0.16	0.01	0.16 ± 0.01	75.3
7.5	0.16	0.13	0.17	0.15	0.01	0.15 ± 0.01	77.0
10	0.13	0.11	0.16	0.13	0.02	0.13 ± 0.02	79.9

3.3. Electrochemical Measurement

3.3.1. Concentration Effect

(i). Open Circuit Potential Measurement

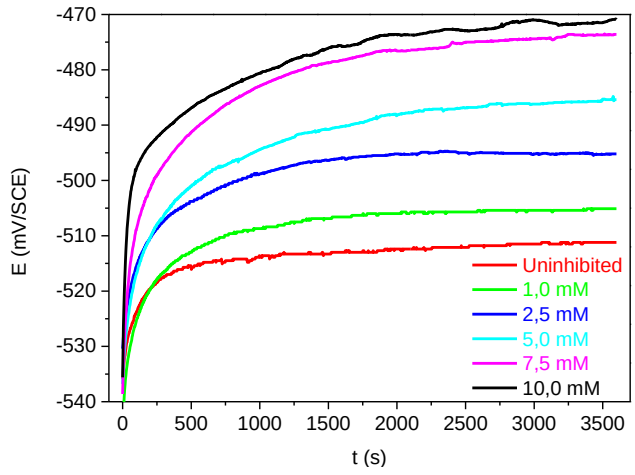

Figure 2. *Zero current chronopotentiometry of C38 steel in the absence and in the presence of different concentrations of PIMP at 30 ℃.*

Open circuit potential (OCP) recording provides preliminary information on the nature of the processes (corrosion, passivation…) occurring at the metal/electrolyte interface and on the required immersion time for the establishment of a stationary regime. The achievement of this equilibrium is mandatory before performing electrochemical impedance and potentiodynamic polarization measurements. [36] The results obtained are presented in Figure 2.

In the molar solution of hydrochloric acid (uninhibited), it can be seen that the OCP of the C38 steel increases sharply during the first 500 seconds due to the active corrosion of the metal. This was followed by a slight and constant increase of the potential due to the gradual stabilization of the corrosion rate. After one hour, the recorded OCP was – 0.511 V/SCE. When different concentrations of PIMP are added, a sharp increase of potential during the first 500 seconds is recorded, followed by a slight and constant increase. This behavior indicates that the presence of PIMP promotes a fast stabilization of the potential at the C38 steel surface. In addition, the OCP curves displayed potentials systematically higher than those recorded without the PIMP in solution, a proof that even minor amounts of this molecule were able to provide valuable protection against steel corrosion. At the end of 1 h, all OCP values measured were in the range -0.505 V to -0.471 V/SCE in the presence of PIMP at concentrations of 1 mM to 10 mM. This suggests a possible modification of the C38 steel surface

by the adsorption of PIMP molecules on the electrode surface. However, a low OCP value gap is noted between concentrations 7.5 mM and 10 mM, involving possible saturation of adsorption sites on the steel surface. 7.5 mM of PIMP can be therefore considered as the optimal concentration. This behavior is close to what was reported by other authors [37-39].

(ii). Electrochemical Impedance Spectroscopy (EIS) Measurements

Figure 3 shows the experimental Nyquist curves, key frequency values, the equivalent circuit model, and the adjusted Nyquist curves (fit data) of C38 steel immersed in 1 M HCl solution (uninhibited) and with the addition of selected PIMP concentrations at 30 ℃ obtained directly after OCP measurement at corrosion potential. The presence of PIMPS in solution increases the diameter of the capacitive loops, indicating an effective protection against C38 steel corrosion.

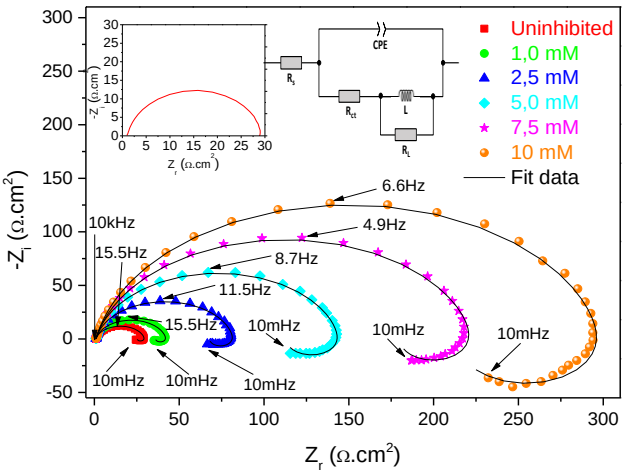

Figure 3. *Nyquist curves of C38 steel in the absence and in the presence of different PIMP concentrations at 30 ℃.*

At high frequencies, the Nyquist diagrams consist of a large capacitive loop. This suggests that the corrosion of C38 steel in 1M HCl medium is mainly controlled by a charge transfer process. At low frequencies, the existence of a small inductive loop is observed, which could be attributed to a process of relaxation of chemical species such as H_3O^+, Cl^- or inhibiting molecules adsorbed on the C38 steel surface or attributed to a redissolution of the passivated surface. [40]

The precise estimation of this corrosion protection ability was based on electrochemical parameters such as: the frequency corresponding to the maximum value of the imaginary component of the Nyquist curve (f_{max}), the surface heterogeneity (n), the constant phase element (CPE), the magnitude of the CPE (Q), the charge transfer resistance (Rct), the solution resistance (R_s), an inductor (L) and inductor resistance (R_L). where L and R_L are associated with the phenomenon of induction at low frequencies. These parameters were obtained upon modelling the metallic interface with suitable equivalent electrical circuits (EEC). The EECS used in this study are presented in Figure 3. This circuit was proposed assuming that one time constant (electric double layer) would govern the processes at the interface, which is consistent with the presence of one inflection point in the corresponding Bode diagrams. These electrical parameters for different experimental conditions are compiled in Table 2 with the calculated standard deviation.

The double layer capacitance was calculated using equation 10: [41]

$$C_{\mathrm{dl}} = \left(\frac{1}{\omega_{\max} R_{\mathrm{ct}}}\right) \tag{10}$$

Where ω_{max} is the maximum angular frequency given by Equation 11: [41]

$$\omega_{\max} = 2\pi.f_{\max} \tag{11}$$

EIS inhibitory efficacy was calculated using equation 12: [42]

$$IE_{\mathrm{EIS}}(\%) = \left(\frac{R_{\mathrm{ct}} - R_{\mathrm{ct}}^{\circ}}{R_{\mathrm{ct}}}\right) \times 100 \tag{12}$$

Where: Rct ° and Rct are the charge transfer resistances without and with inhibitor, respectively.

The values of the relaxation time constant (t) of the charge transfer process are obtained using Equation 13: [43]

$$t = R_{\mathrm{ct}} C_{\mathrm{dl}} \tag{13}$$

The parameters used in equations 10 to 13 are defined above.

According to Table 2, the values of Rct increase, and those of Q and Cdl decrease with the addition of the PIMP to the corrosive solution. This can be ascribed to the formation of a protective layer at the metal/acid interface, thus decreasing the direct contact between the C38 steel and the aggressive solution. [44] In addition to this, the increasing value of the inhibition efficiency in the presence of PIMP further supports the protection ability of the inhibitor.

The values of the (t) increase when PIMP concentrations are added to a corrosive solution. The adsorption process time becomes important, indicating that the adsorption process in the presence of the inhibitor is slow. [43] However, regarding the same (t) values and low inhibition efficiency gap between 7.5 mM and 10 mM concentrations, it can therefore be assumed that 7.5 mM of PIMP is the optimal concentration as seen with OCP measurements.

Table 2. *EIS parameters and inhibition efficiency at 30 ℃ of C38 steel in the absence and in the presence of different concentrations of PIMP.*

C (mM)	Rct ($\Omega.cm^2$)	Q ($\mu\Omega^{-1}.Sn.cm^2$)	n	C_{dl} ($\mu F.cm^{-2}$)	T (s)	IE_{EIS} (%)
Blank	23.1 ± 1.6	634.6 ± 19.3	0.876 ± 0.003	406.8	0.009	/
1.0	39.7 ± 4.6	535.1 ± 91.2	0.874 ± 0.019	334.6	0.013	38.7
2.5	65.8 ± 1.2	286.5 ± 2.8	0.902 ± 0.000	210.3	0.014	63.0
5.0	91.3 ± 20.9	223.1 ± 14.6	0.887 ± 0.013	200.7	0.018	73.3
7.5	193.0 ± 13.9	174.6 ± 21.6	0.887 ± 0.005	143.6	0.028	87.4
10.0	204.4 ± 8.0	155.1 ± 21.1	0.876 ± 0.013	135.6	0.028	88.1

Figure 4 (a, b) shows the Bode plots: (a) logarithm of impedance modulus $|Z|$ versus logarithm of frequency and (b) phase shift $\emptyset$ versus logarithm of frequency for C38 steel without and with the presence of different concentrations of PIMP at 30 ℃:

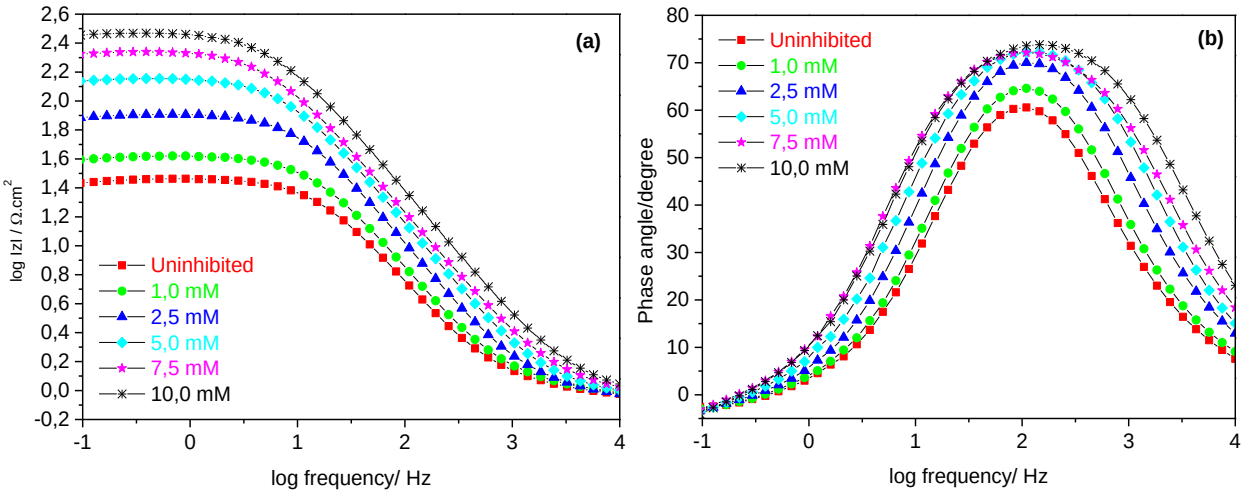

Figure 4. *Bode diagram: impedance modulus (a), phase angle (b) of C38 steel in the absence and in the presence of different PIMP concentrations.*

Increasing the concentration of the inhibitor leads to an increase in $\log|Z|$ and phase angle $\emptyset$. The appearance of a single drop in (a) or a single peak in (b) for uninhibited and all concentrations studied, the detection of a single time constant at the metal/electrolyte interface takes this into account. [45]

(iii). Potentiodynamic Polarization (PDP) Measurements

In order to evaluate the impact of PIMP molecules on the evolution of cathodic and anodic reactions on the surface of C38 steel, Figure 5 shows the polarization curves recorded at 30 ℃ in 1 M HCl medium in the absence and in the presence of PIMP concentrations.

The addition of the inhibitor decreases the anodic dissolution and delays the hydrogen ion reduction reaction. This addition shows the shape of almost parallel cathodic Tafel branches. This indicates that the mechanism of hydrogen evolution, mainly due to charge transfer as seen with EIS data, is not modified upon addition of the inhibitor.

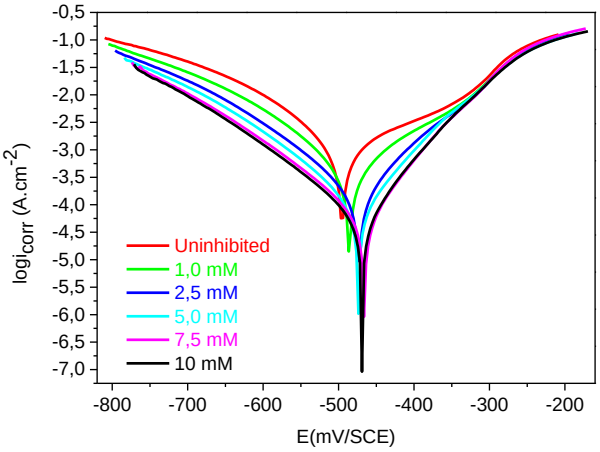

Figure 5. *Polarization curves of C38 steel in the absence and in the presence of different concentrations of PIMP at 30 ℃.*

The mechanism of hydrogen evolution is shown by equations 14-16: [46]

$$Fe + H^+ \leftrightarrow (FeH^+)_{ads} \quad (14)$$

$$(FeH^+)_{ads} + e^- \rightarrow (FeH)_{ads} \quad (15)$$

$$(FeH)_{ads} + H^+ + e^- \rightarrow Fe + H_2 \quad (16)$$

The addition of PIMP generates a change of anodic Tafel slope. This inhibitor is adsorbed on the surface of the metal before blocking the active sites without modifying the anodic dissolution mechanism, which is shown by equations 17-20: [47]

$$Fe + Cl^- \leftrightarrow (FeCl^-)_{ads} \quad (17)$$

$$(FeCl^-)_{ads} \leftrightarrow (FeCl)_{ads} + e^- \quad (18)$$

$$(FeCl)_{ads} \rightarrow (FeCl^+)_{ads} + e^- \quad (19)$$

$$(FeCl^+)_{ads} \rightarrow Fe^{2+} + Cl^- \quad (20)$$

An increase in current is also observed for potentials above 350 mV/SCE in most of the anodic curves. This could be due to the desorption of molecule inhibitors from the steel surface.

PDP parameters, namely, corrosion potential (Ecorr), anodic and cathodic Tafel slopes (ba and bc), corrosion current (icorr), and polarization resistance (Rp) obtained by extrapolation of the polarization curves are grouped in table 3.

One can note a shift in the corrosion potential in presence of different PIMP concentrations compared to the blank corrosion potential. This shift being less than 85 mV/SCE, suggesting that this compound acts as a mixed-type inhibitor. The polarization resistance significantly increases and the corrosion current decreases with the increased of PIMP's concentration, which implies that PIMP molecules act by inhibiting the corrosion activity of C38 steel. Inhibition efficiency (IE%) calculated from Rp or icorr are the same values. It could be explained by the good Tafel fit. IERp (%) increases with concentration and reaches a maximum of 91.7% at 10mM of PIMP. This assumes that the action of the inhibitor is due to adsorption on the steel surface. However, a slight difference is observed in the inhibition percentage for 7.5mM and 10mM concentrations. This indicates a saturation of the adsorption sites on the C38 steel surface. 7.5mM can be considered as an optimal concentration as already observed in the OCP and SIE techniques. Figure 6 shows the column data of inhibition efficiency obtained using EIS and PDP techniques as a function of PIMP concentration.

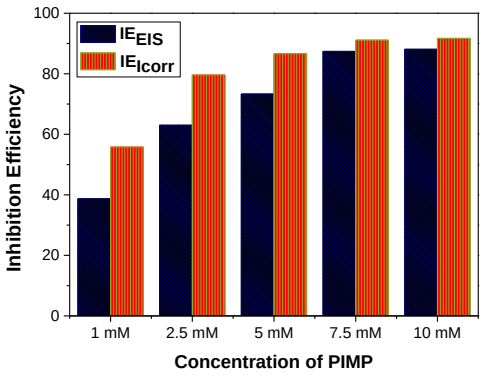

Figure 6. *Evolution of inhibition percentage with PIMP concentration using EIS and PDP techniques.*

For each concentration of PIMP, the values of IE_{EIS} are low compared to IE_{Icorr}. Gap values ($\Delta E = IE_{Icorr} - IE_{EIS}$) decrease when the PIMP concentration increases.

Even throw, one cannot exclude some experimental errors during the recording of the use of the curves and adjustment of the data, this evolution could be due to the fact that the EIS technique, being more sensitive, would give more ideal values of IE% compared to the PDP technique. where Tafel approximation may overestimate the inhibitory efficacy of the PIMP. Moreover, a decrease in ΔE is observed with the concentration, which could be explained by the better sensitivity of the PDP technique when the inhibition efficiency already reaches its optimum.

Table 3. *Electrochemical parameters and inhibitory efficiencies obtained from LSV curves of C38 steel in 1M HCl at different PIMP concentrations at 30 ℃.*

C (mM)	Ecorr (mV/SCE)	Rp (Ohm)	Icorr (μA/cm^2)	Ba (mV/dec)	Bc (mV/dec)	IE_{Rp} (%)	IE_{Icorr} (%)
Blank	-493.4 ± 1.0	27.9 ± 3.9	1203.4 ± 200.6	192.0 ± 14.0	128.3 ± 1.4	/	/
1.0	-482.4 ± 2.9	52.6 ± 1.4	498.2 ± 18.0	123.2 ± 8.1	115.0 ± 3.5	55.7	55.8
2.5	-473.2 ± 0.6	117.5 ± 0.5	173.9 ± 1.1	85.1 ± 0.1	105.4 ± 0.7	79.6	79.6
5.0	-473.7 ± 0.4	157.0 ± 21.0	130.3 ± 20.3	80.2 ± 1.5	102.8 ± 2.2	86.6	86.6
7.5	-468.6 ± 1.2	237.5 ± 30.5	79.8 ± 13.1	71.4 ± 2.9	101.4 ± 0.1	91.1	91.1
10.0	-470.2 ± 0.0	289.0 ± 0.0	63.8 ± 0.0	70.1 ± 0.0	102.8 ± 0.0	91.7	91.7

3.3.2. Temperature Effect

The temperature of the system is one of the important factors in the study of corrosion inhibition for steel in aggressive environment. In order to determine the effect of this variable on the inhibitory performance of PIMP, we carried out electrochemical tests at different temperatures: 10 ℃, 20 ℃, 30 ℃, 40 ℃, 50 °C and 60 °C. Different PIMP concentrations were also investigated: 1.0mM, 2.5mM, 5.0mM, and 7.5mM. Figure 7 shows the effect of temperature on the Linear Sweep Voltammetry (LSV) curves obtained in 1M HCl medium containing different PIMP concentrations:

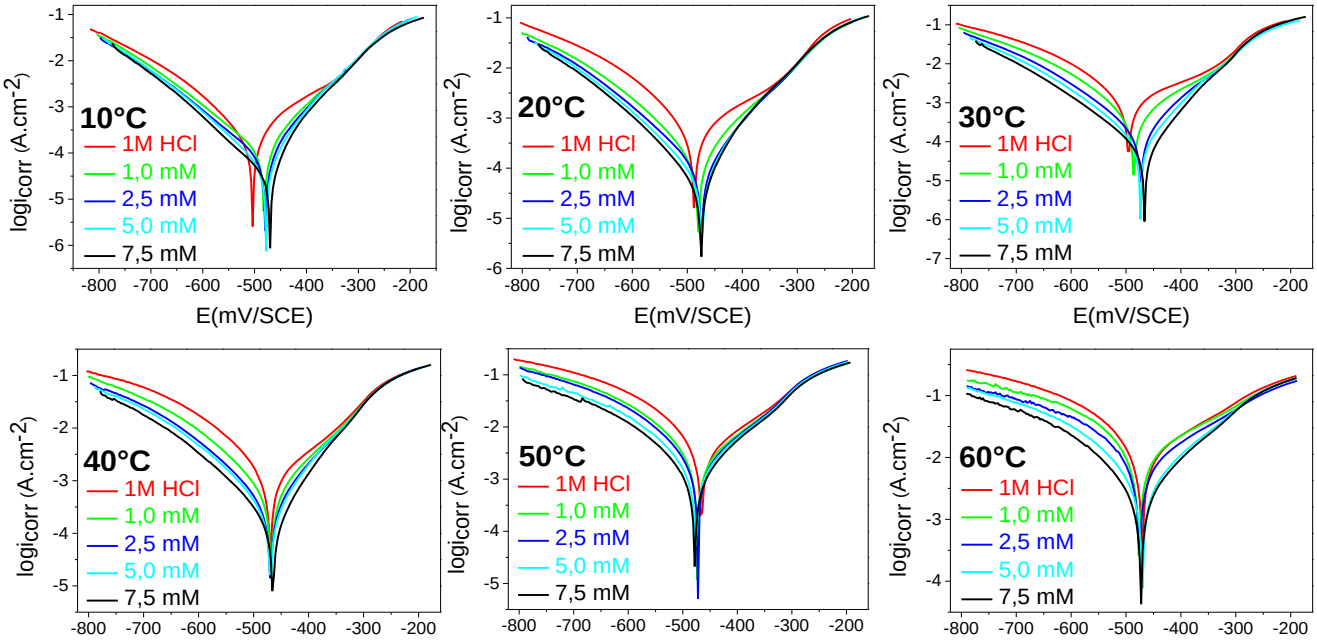

Figure 7. *Linear sweep voltammetry curves of C38 steel at different PIMP concentrations and temperatures.*

For all temperatures studied, the ΔEcorr between the blank and each PIMP concentration remains lower than 85mV/SCE. The cathodic and anodic branches in the presence of different concentrations are lowered compared to that of 1M HCl (blank), this implies that PIMP remains a good mixed-type inhibitor. It is also noted that the desorption potential (-350mV/SCE) is not modified with the increase in temperature.

The electrochemical parameters obtained according to the different ranges of temperature and concentration are grouped in Table 4. For each blank and for each PIMP concentration, it is observed that the increase in temperature also leads to an increase in corrosion current and to a decrease in polarization resistance. This confirms the dissolution of the metal with increasing the temperature. Despite this increase, the corrosion current decreases with rising inhibitor concentration for each temperature. This suggests that PIMP remains a suitable inhibitor.

Figure 8 presents the evolution of the inhibitory effectiveness as a function of temperature and concentration. The inhibitory efficiency (IE) increases with the concentration; however, with temperature, we note that IE increases when moving from 10 ℃ to 30 ℃ and decreases when moving from 30 ℃ to 60 ℃. This evolution could be explained by the fact that the adsorption of PIMP molecules on the C38 steel surface is sensitive to heat and this adsorption becomes unstable as one moves away from the ambient temperature. Thus, 30 ℃ is the optimal temperature for optimal inhibitory efficacy.

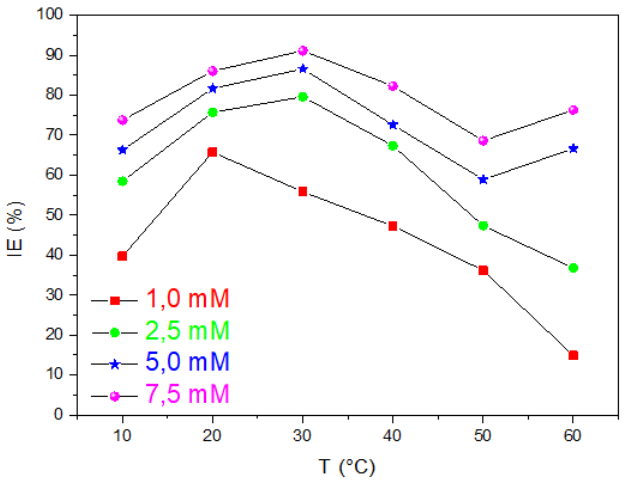

Figure 8. *Evolution of the inhibitory efficacy of PIMP as a function of temperature and concentration.*

Table 4. *Electrochemical parameters obtained from polarization curves of C38 steel in 1M HCl medium with addition of PIMP at different temperatures.*

T (℃)	C (mM)	E_{corr} (mV/SCE)	R_p (Ohm)	i_{corr} (µA.cm-2)	b_a (mV.dec-1)	b_c (mV.dec-1)	IE_{Rp} (%)	IE_{LSV} (%)
10	Blank	-504.8	102.0	268.1	152.9	94.1	/	/
	1.0	-483.2	155.0	161.6	105.2	117.8	34.2	39.7
	2.5	-480.9	213.0	105.8	90.7	113.8	52.1	58.5
	5.0	-480.6	285.0	85.9	95.0	102.0	64.2	66.3
	7.5	-474.3	368.0	66.9	94.3	93.6	72.3	73.7
20	Blank	-486.7	45.0	585.6	124.5	137.7	/	/
	1.0	-480.8	128.0	200.6	100.7	116.1	65.1	65.7
	2.5	-474.8	183.0	142.3	88.3	119.4	75.6	75.7
	5.0	-475.2	243.0	107.3	89.7	106.9	81.6	81.7
	7.5	-477.1	317.0	81.7	84.6	102.3	85.9	86.0
30	Blank	-494.5	23.9	1092.3	182.5	117.5	/	/
	1.0	-485.3	54.0	482.6	131.7	110.1	55.7	55.8
	2.5	-473.8	117.0	223.1	93.8	113.4	79.6	79.6
	5.0	-474.1	178.0	146.6	82.8	110.0	86.6	86.6
	7.5	-467.3	268.0	97.1	75.9	109.9	91.1	91.1
40	Blank	-468.9	19.1	1357.4	100	149.7	/	/
	1.0	-468.5	36.4	716.3	99.7	132.9	47.5	47.2
	2.5	-470.0	58.4	443.3	92.8	125.1	67.3	67.3
	5.0	-469.9	70.2	372.3	88.1	123.5	72.8	72.6
	7.5	-466.0	108.0	240.9	81.2	117.8	82.3	82.3
50	Blank	-464.2	6.4	4093.7	136.9	147.9	/	/
	1.0	-471.9	10.0	2613.3	124.5	148.3	35.9	36.2
	2.5	-471.4	12.1	2155.7	119.6	141.8	47.1	47.3
	5.0	-475.8	15.5	1682.8	123.8	134.3	58.7	58.9
	7.5	-477.5	20.3	1285.5	117.5	131.1	68.5	68.6
60	Blank	-469.3	2.4	11026.3	189.5	155.7	/	/
	1.0	-475.3	2.7	9389.4	197.6	148.6	12.9	14.8
	2.5	-474.3	3.7	6974.5	186.5	146.3	35.6	36.7
	5.0	-469.8	7.0	3679.5	137.5	138.7	66.0	66.6
	7.5	-472.7	9.5	2614.6	129.5	133.2	75.1	76.3

3.4. Thermodynamic Activation Parameters

3.4.1. Activation Energy

The Arrhenius relationship (equation 21), between the corrosion current and the temperature, made it possible to calculate the activation energies of the corrosion process of C38 steel immersed in 1M HCl medium at different PIMP concentrations (0mM, 1mM, 2.5mM, 5mM and 7.5mM): [48]

$$\ln(i_{corr}) = -\frac{E_a}{R} \times \frac{1}{T} + \ln K \quad (21)$$

Where icorr (A.cm^{-2}): corrosion current intensity; K: constant (pre-exponential factor), Ea (kJ.mol^{-1}): activation energy; R = 8.314 J.mol^{-1}.K^{-1}: perfect gas constant and T (Kelvin): temperature.

Activation energy values are obtained using the slopes of the lines. The graphical representations of ln(icorr) as a function of (1/T) in the absence and in the presence of PIMP at different concentrations are presented in Figure 9:

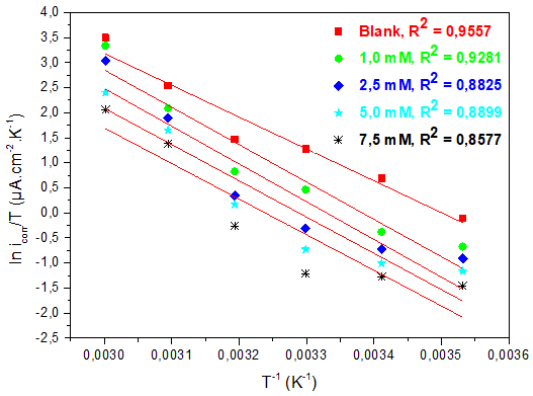

Figure 9. *Arrhenius straight lines obtained from corrosion current density of C38 steel and with different PIMP concentrations to obtain Ea.*

The values of the activation energy without and in the presence of the inhibitor are grouped together in Table 5. The literature specifies that the inhibitors whose activation energy is greater than that without the inhibitor $E_a^{inh} < E_a$ adsorb on the substrate (C38 steel) by electrostatic bonds (physisorption) and the inhibitors of which $E_a^{inh} < E_a$ are adsorbed on the surface of the metal via strong bonds (chemisorption). [45, 49] In our case, the values of E_a^{inh} are all higher than those in the absence of the inhibitor: the PIMP molecules are therefore physiosorbed on the C38 steel surface. This can be correlated to the evolution of inhibition efficacy as seen in Figure 8.

3.4.2. Standard Enthalpy of Activation and Standard Entropy of Activation

An alternative formula (equation 22) of the Arrhenius equation is used to determine the standard enthalpy of activation and the standard entropy of activation: [46]

$$\ln\left(\frac{i_{corr}}{T}\right) = -\frac{\Delta H_a^\circ}{R} \times \frac{1}{T} + \ln\left(\frac{R}{N.h}\right) + \frac{\Delta S_a^\circ}{R} \quad (22)$$

Where: h= 6.63.10-34 Js: Planck's constant; N= 6.022.1023 mol^{-1}: Avogadro's number; R = 8.314 J.mol^{-1}. K^{-1}: perfect gas constant; ΔHa° (kJ.mol^{-1}): standard enthalpy of activation; ΔSa° (J.mol^{-1}.K^{-1}): Standard entropy of activation.

The slopes of the straight lines are used to find the values of the standard enthalpy of activation and the intercept permits to calculate the standard entropy of activation. The variations of $\ln(i_{corr}/T)$ as a function of (1/T), at different PIMP concentrations are illustrated in figure 10:

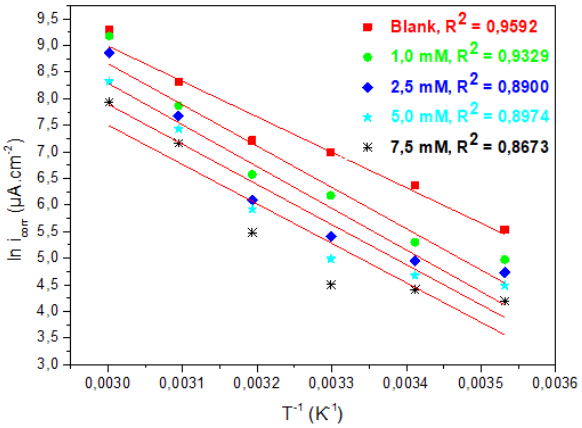

Figure 10. *Arrhenius straight lines obtained from corrosion current density of C38 steel at different concentrations of PIMP for obtain ΔHa° and ΔSa°.*

The exploitation of all these straight-line equations made it possible to find the values of ΔHa°; and ΔSa° recorded in Table 5:

Table 5. *Activation parameters obtained in 1M HCl medium in the absence and in the presence of different concentrations of PIMP for C38 steel.*

C (mM)	E_a (kJ.mol^{-1})	ΔH_a° (kJ.mol^{-1})	ΔS_a° (J.mol^{-1}.K^{-1})
Blank	55.46	52.91	-12.3
1.0	64.22	61.67	11.05
2.5	64.97	62.42	10.28
5.0	61.52	58.97	-3.74
7.5	61.04	58.49	-8.22

The positive values of ΔHa° reflect the endothermic nature of the C38 steel dissolution and inhibition process. This has also been reported to be indicative of retarded dissolution of metals in inhibitor-containing solution [6]. Negative signs of ΔSa° in the absence and presence of 5.0mM and 7.5 mM of PIMP means that the activated molecules were in a lower order state compared to the initial step [45]. For 1.0mM and 2.5mM, the standard entropy of activation ΔSa° is positive; this implies that the activated molecules were in a higher order state compared to the initial step. The values of the standard entropy of activation ΔSa° in the presence of different PIMP concentrations are higher than in the absence of inhibitor, thus there is an increase in the disorder during the adsorption process [49]. However, for different concentrations of inhibitor, a decrease in the standard entropy of activation is observed when the PIMP concentration increases. This indicates a reduction in disorder, implying a higher stability of the protective layer on the C38 steel surface and the formation of the Fe-PIMP complex [2].

Additional information regarding the corrosion inhibition mechanism of steel can be obtained by studying the adsorption parameters.

3.5. Adsorption Isotherm Model

In order to have more ample information concerning the mode of interaction between the inhibitor and the metal surface, adsorption isotherm models were studied. Among the models of adsorption isotherms, Langmuir model isotherm was found to be in agreement with our results.

In this model, the relationship between the fraction of covered sites on the steel surface (θ) and the concentration of the inhibitor (Cinh) is given by equation 23: [50]

$$\frac{C_{\text{inh}}}{\theta} = \frac{1}{K_{\text{abs}}} + C_{\text{inh}} \quad (23)$$

With K_{abs}: Equilibrium constant of the adsorption process.

The variations of the C_{inh}/θ (mM) ratio as a function of the concentration of extract for each temperature are presented in Figure 11:

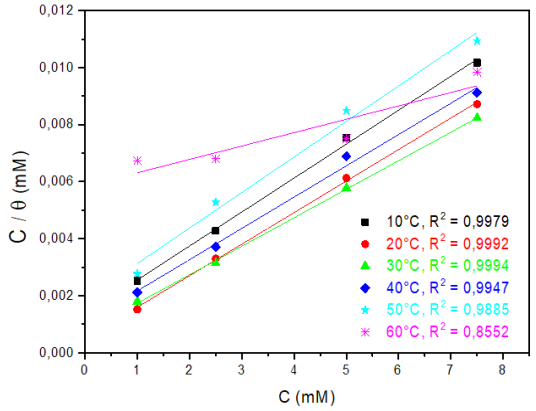

Figure 11. *Langmuir isotherm model for C38 steel in 1M HCl solution in the presence of PIMP at different temperatures.*

The validity of the Langmuir equation is confirmed by the linearity of C_{inh}/θ (mM) as a function of the concentration of the inhibitor with a correlation coefficient close to unity. In relation to the R_2 values, the adsorption of PIMP on the C38 steel surface in 1M HCl solution obeys the Langmuir isotherm. The inhibition is surely due to the formation of a single layer on the metal surface, limiting the access of the electrolyte to the surface of C38 steel.

The Gibbs standard adsorption energy ($\Delta G_{ads}°$) and the equilibrium constant of the adsorption process (K_{ads}) are linked by equation 24: [6]

$$\Delta G^{\circ}_{\text{ads}} = -RT \ln(55{,}5 \times K_{\text{ads}}) \quad (24)$$

Where R is the ideal gas constant, T is the temperature, and 55.5 is the concentration of water in solution (mol/L).

The standard adsorption enthalpy ($\Delta H_{ads}°$) and the standard adsorption entropy ($\Delta S_{ads}°$) were calculated using equation 25: [51]

$$\Delta G_{ads}° = \Delta H_{ads}° - T\Delta S_{ads}° \quad (25)$$

Where $\Delta H_{ads}°$ and $\Delta S_{ads}°$ are, respectively, the intercept and the negative slope of the plot of ΔGads° as a function of T.

Table 6. *Thermodynamic parameters of adsorption of PIMP on C38 steel at different temperatures.*

T (℃)	R2	Kads (M-1)	$\Delta G^{\circ}_{\text{ads}}$ (kJ.mol-1)	$\Delta H^{\circ}_{\text{ads}}$ (kJ.mol-1)	$\Delta S^{\circ}_{\text{ads}}$ (J.mol-1K-1)
10	0.9979	714.29	-41.19	-27.2	57.4
20	0.9992	2000.00	-45.15		
30	0.9994	1428.57	-45.84		
40	0.9947	909.09	-46.18		
50	0.9885	526.32	-46.18		
60	0.8552	172.41	-44.52		

Table 6 displays the values of thermodynamic parameters of adsorption. A negative ΔGads° implies a spontaneous adsorption process. [11] A positive ΔS_{ads} ° shows that the entropy of the solvent (H_2O) prevails over the entropy of the solute (PIMP). [10] A negative ΔH_{ads} ° implies that the adsorption process is exothermic. However, the adsorption mode of corrosion inhibitors is often determined by criteria based on the standard free energy of adsorption, with values greater than 20 kJ/mol attributed to physisorption and values smaller than 40 kJ/mol attributed to chemisorption [52-54] According to (Anton Kokalj, 2022), [55] Several arguments are presented here to show that these are not very reliable criteria to distinguish between physisorption and chemisorption. This can be done through computational modeling studies. [55]

3.6. FESEM /EDX Analysis

The Field Emission Scanning Electron Microscopy (FESEM) and Energy Dispersive X-ray (EDX) mapping obtained from the C38 steel samples after 5 hours in 1M HCl solution, in the absence and in the presence of 5mM PIMP are presented in figure 12. In the absence of inhibitor, Figure 12 (a), a strong degradation of the steel surface is observed with the formation of non-uniformly distributed oxide layer. This is probably related to the oxidation of iron in the presence of chloride ions. [56] Of fact, it is known that the presence of aggressive anions such as chloride ions leads to the remove of the passive oxide layer present on the metal surface. The degradation of the metal is more important compared to the rest of the steel surface. Elementary EDX mapping of the steel surface obtained under the same conditions highlights the presence of a formed oxide layer, likely attributable to the uniformly distribution of oxygen on the surface. We also note a weak coloration on the elemental mapping of chlorine, proof of the significant presence of chloride ions on the C38 steel surface. Figure 12 (b) shows the surface condition of C38 steel in the presence of 5mM PIMP. Compared with Figure 12 (a), there is a surface uniformity due to the adsorption of PIMP molecules on the steel surface [57], Contrary to the first analyzed case, we observed a strong uniform coloration of oxygen and chlorine on the surface of the steel. This state is probably due to the uniform adsorption of PIMP molecules containing oxygen atoms leading to a complex with Fe(II) and Cl^- ions [36].

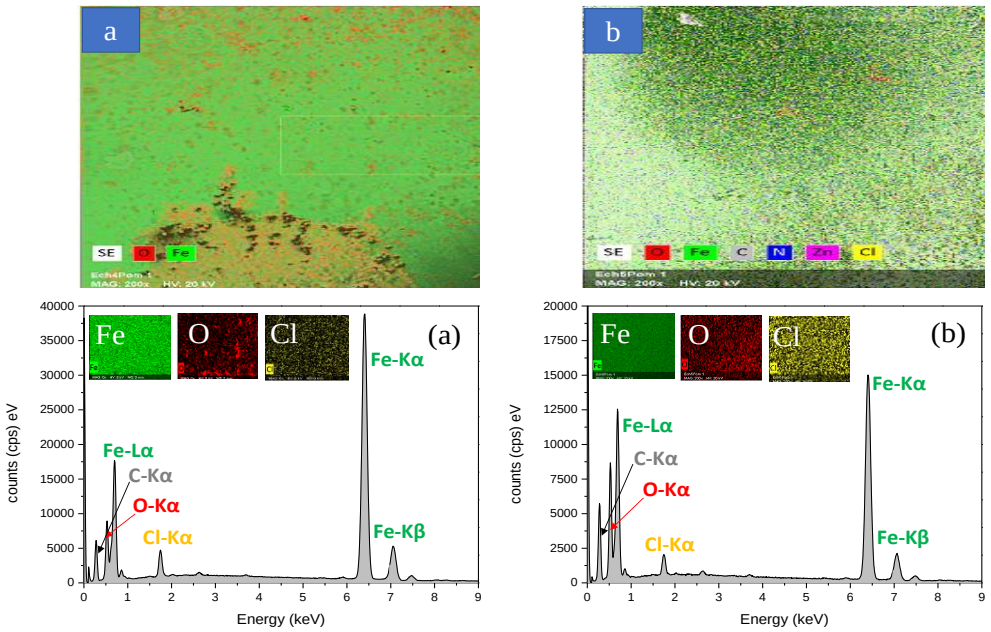

Figure 12. *FESEM/EDX mapping of the C38 steel surface in 1M HCl solution without inhibitor (a), and in the presence of 5mM PIMP (b).*

3.7. Quantum Chemical Calculation

3.7.1. Frontier Molecular Orbitals (FMO) and Mulliken Atomic Charge (MAC)

The geometry of PIMP inhibitor and its protonated form were optimized at the Becke-3-parameter Lee–Yang–Parr (B3LYP) level with the 6-31G (d, p) basis in the gaseous phase. It should be mentioned that the protonated form of the inhibitor corresponds to the system in which the nitrogen atom is tetravalent as seen in Figure 13. With the optimized geometry, visual observation of the optimized molecule configuration shows that this molecule is almost flat. This allows us to predict that PIMP has an almost planar or parallel layout on the surface of the C38 steel. The frontier molecule

orbitals (highest occupied and lowest unoccupied molecular orbitals (HOMO and LUMO)) were directly obtained. The molecular electrostatic potential maps and the Mulliken charge distribution were also straight forwarded obtained from the geometrical structure and shown in Figure 14. Inspection of Figure 13 indicates that the electronic density of HOMO and LUMO is distributed over the whole skeleton of PIMP and its protonated form. Moreover, the energy gap value of PIMP is greater than its protonated form ($PIMPH^+$), implying that the neutral form would have the greatest electron density. This shows that this compound possesses several active sites distributed along the molecular structure, allowing electrons to be donated to vacant orbitals of the Fe-surface or a back-donation interaction between the inhibitor and the Fe-surface and leading to increased adsorption efficiency of the tested inhibitor.

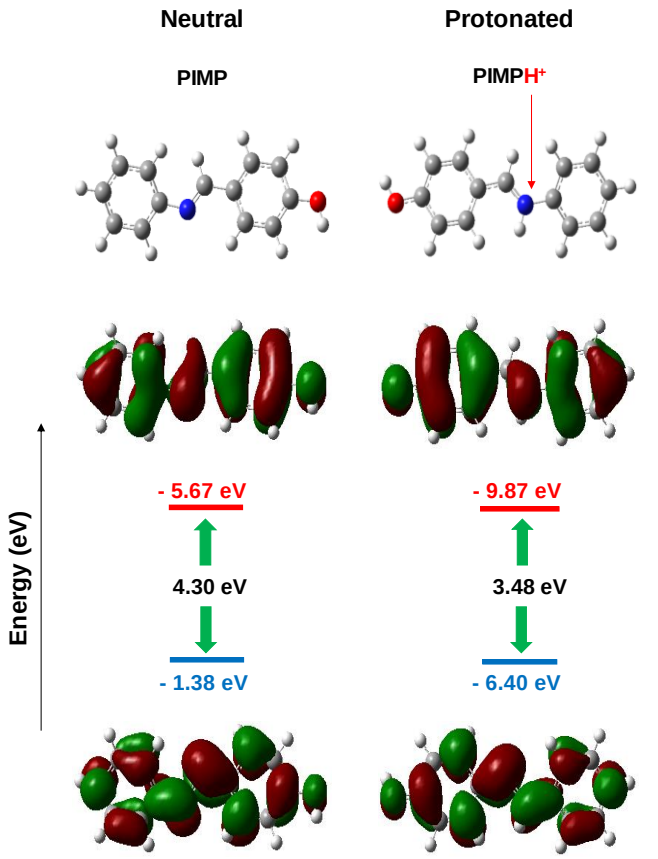

Figure 13. *Optimized structure (upper), HOMO (red) and LUMO (blue) energy levels, and the number (black) on the arrows (green) is its energy gap of the investigated inhibitor (PIMP) and its protonated form, and the 3D distributions of HOMO (middle) and LUMO (lower) orbitals of the neutral form and the protonated form of PIMP inhibitor. The results were obtained at the B3LYP/6-31G(d,p) level in the gaseous phase.*

These results are also confirmed when the distribution of the total density mapped to the electrostatic potential (MEP) as represented in Figure 14. The gradual decreasing in the electron density is indicated by the ranged colors (from red to blue). Additionally, the Mulliken atomic charge distributions on C, H, O, and N atoms in the investigated inhibitor are also shown in Figure 14, together with their grade color. Visual examination of this figure reveals that protonation can alter the electron density repartition. As can be seen in Figure 14, O and N atoms in both forms (neutral and protonated) have the highest negative charge, as well as aromatic ring carbon atoms, confirming their tendency to donate electrons. The results show that the protonated form has de highest negative charge. These results indicate that Schiff bases are excellent corrosion inhibitors in acidic environments, compared to neutral or alkaline chloride media.

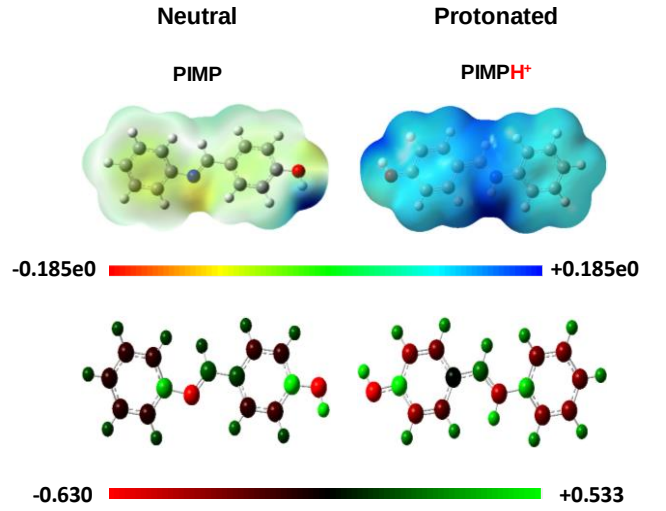

Figure 14. *(Upper)Electrostatic potential maps and (Lower) the Mulliken atomic charge distribution of the studied inhibitor molecule (PIMP) in its neutral form and protonated form at the B3LYP/6-31G(d,p) level in gaseous phase.*

3.7.2. Global Reactivity Descriptor

Global quantum parameters estimated based on the E_{HOMO} and E_{LUMO} values of the optimized structure are calculated four times and the mean values with standard deviation are listed in Table 7. These descriptors are used to explain the basic properties of PIMP inhibitors and to demonstrate the interaction with the metal surface.

Table 7. *Calculated Quantum descriptors of the PIMP inhibitor in its neutral (PIMP) and protonated ($PIMPH^+$) form at the B3LYP/6-31G(dp) level in gaseous phase.*

Quantum descriptors	Neutral form		Protonated form	
	Average Values	Standard deviation	Average Values	Standard deviation
μ (D)	1.3910	0.0024	1.9710	0.0001
E_{HOMO} (eV)	-5.6719	0.0003	-9.8725	0.0003
E_{LUMO} (eV)	-1.3761	0.0032	-6.3950	0.0002
ΔE_{gap} (eV)	4.2957	0.0031	3.4775	0.0005
η (eV)	2.1479	0.0016	1.7387	0.0003
σ (eV-1)	0.4656	0.0003	0.5751	0.0001
χ (eV)	3.5240	0.0016	8.1338	0.0001
ω (eV)	0.4506	0.0015	1.1171	0.0002
ΔN	3.7330	0.0044	-0.9857	0.0002

The corrosion inhibiting performance of a compound depends on its structure, the type of metal, and the nature of the aggressive medium. The choice to use PIMP molecules as a corrosion inhibitor is justified by the fact that it has in its structure a conjugated system of π bonding to the benzene nucleus, heteroatoms (O and N), all capable of repelling the molecules of water adsorbed on the surface of the electrode. [58] A high value of E_{HOMO} of an inhibitor molecule implies its facility to donate electrons to the empty or unoccupied orbitals of the metal. On the other hand, if E_{LUMO} is low, the molecule easily captures the electrons of the metal. Therefore, a low value of ΔE implies a better inhibitory efficacy. [59] The dipole moment (μ) can also be used to assess the adsorption capacity of the inhibitor. Some results show that a larger μ is responsible for a greater inhibition efficiency. [60] As expected, an inspection of Table 7 indicates that ΔE ($PIMPH^+$) < ΔE (PIMP) and μ (PIMP) < μ ($PIMPH^+$) imply that the protonated form has a better inhibition compared to its neutral form, as view in FMO and MAC section. Figure 14 shows that PIMP can interact with the iron surface via a donor-acceptor adsorption model of its different groups. Indeed, the hydroxyl group and azomethine have free electron pairs which can lodge in the empty "d" orbitals of the metal. The π* orbitals of the benzene nucleus accept electrons from the iron "3d" orbitals during feedback donation.

ΔN can be used to evaluate the fraction of electrons transferred from the inhibitor molecule to the surface of C38 steel. It is obtained using equation 26: [61]

$$\Delta N = \chi_{Fe} - \chi_{inh(PIMP)} / \left[2\left(\eta_{Fe} + \eta_{inh(PIMP)}\right)\right] \quad (26)$$

Where: $\chi_{inh(PIMP)}$ is the electronegativity and $\eta_{inh(PIMP)}$ is the hardness of the PIMP molecule, obtained using equations 27 and 28: [62]

$$\chi = (I + E)/2 \quad (27)$$

$$\eta = (I - E)/2 \quad (28)$$

The ionization potential (I), electron affinity (E), overall softness (σ) and electrophilic character (ω) of the molecule are calculated using equations 29-32: [46]

$$I = -E_{HOMO} \quad (29)$$

$$E = -E_{LUMO} \quad (30)$$

$$\sigma = 1/\eta \quad (31)$$

$$\omega = \mu^2/2\eta \quad (32)$$

Where $\chi_{Fe} = 7\ eV.mol^{-1}$, and $\eta_{Fe} = 0\ eV.mol^{-1}$ f or iron.

Moreover, ΔN > 0, the electrons transferred from the inhibitor to the metal are predominant. ΔN < 0, the electrons will rather be transferred from the metal surface to the inhibitor. [63] ΔN ($PIMPH^+$) = -0.9857, shows that the electron transfer occurs mainly from the steel surface to the inhibitor molecule.

The Hard and Soft Acid-Base theory suggested by Pearson states that a hard acid reacts preferentially with a hard base, while a soft acid prefers to interact with a soft base. This theory could be applied to choose appropriate inhibitors and to assess the effectiveness of inhibitors. [64] Fe(II), is considered as a soft acid, and therefore prefers to interact with soft bases which easily give up their electron pairs to the metal. Consequently, an effective inhibitor should have a high soft-

ness σ (inhibitor ability to give up its electrons) and a low hardness η (inhibitor ability to retain its electrons). Looking at the values in Table 7, the protonated form of PIMP is a good corrosion inhibitor and has a strong interaction with the metal surface. The calculated electronegativity (χ) and electrophilicity (ω) values of the PIMP molecule showed a strong ability to transfer electrons from PIMP to the metal surface. [65]

3.7.3. Fukui Function and the Local Dual Reactivity Indices

The numbering of atoms is given in Figure 15.

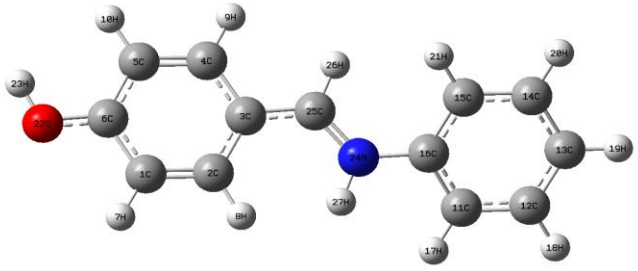

Figure 15. *Optimized $PIMPH^+$ structure showing labels and symbols.*

For the PIMP (neutral form), the highest nucleophilic attack sites (f_k^+) are C6 and C5, while the highest electrophilic attack sites (f_k^-) are C13 and C14.

The estimated values of the dual descriptors, which are shown in Table SI2 of the supplementary information summary, allow us to instantly find the preferable sites for nucleophilic attacks $(f_k^2, \Delta\omega_k \; and \; \Delta\sigma_k > 0)$ and the preferable sites for electrophilic attacks $(f_k^2, \Delta\omega_k \; and \; \Delta\sigma_k < 0)$ over the system at point k. [66, 67]

Figure 16 shows the dual descriptors: $f_k^2, \Delta\omega_k \; and \; \Delta\sigma_k$ of the neutral form of PIMP compound. As shown by the condensed Fukui functions and the local softness and philicity, the neutral form of PIMP has only four most active sites which are only a few carbon atoms from the aromatic rings. According to Figure 16, one concludes that the most active sites that can react with the iron surface in the PIMP compound by donating electrons, are some carbon atoms (C5 and C6) of the benzaldehyde ring.

Whereas, the carbon atoms of the aniline ring are the site to accept electrons from Fe surface to form back-bonding interaction. Figure 17 shows the dual descriptors: $f_k^2, \Delta\omega_k \; and \; \Delta\sigma_k$ of the protonated form of PIMP compound. According to this figure, protonation changes the active sites of PIMP, compared to the neutral form. These changes could be attributed to electron shifts by the mesomeric effect. According to these descriptors, one concludes that the only site that can react with the iron surface in the protonated form of PIMP by donating electrons is the carbon atom (C6) of the benzaldehyde ring. The back-bonding interaction is assumed by the carbon atom (C3) of the benzaldehyde ring. These results are in agreement with those obtained by HOMO, LUMO, and ESP maps.

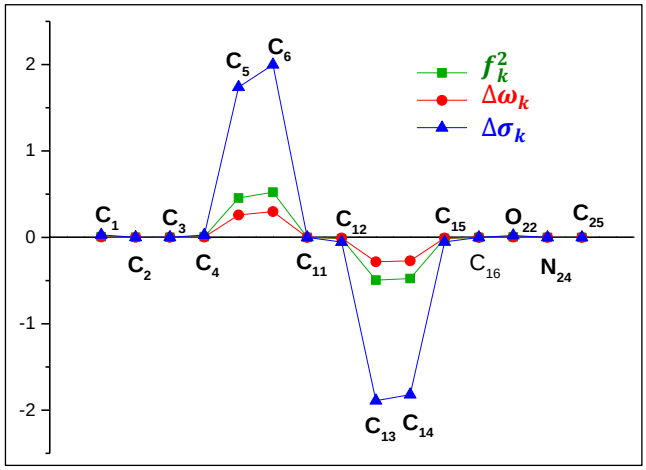

Figure 16. *The condensed local dual descriptors $(f_k^2, \Delta\omega_k \; and \; \Delta\sigma_k)$, based on Fukui Functions of PIMP inhibitor in its neutral form as obtained using DFT/B3LYP/6-311G(d,p) method.*

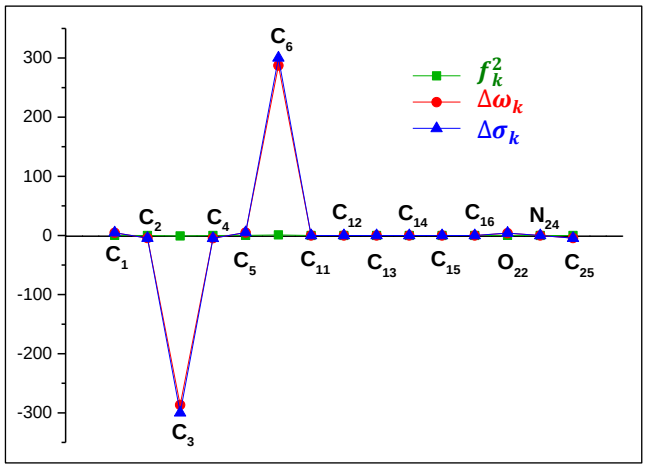

Figure 17. *The condensed local dual descriptors $(f_k^2, \Delta\omega_k \; and \; \Delta\sigma_k)$, based on Fukui Functions of PIMP inhibitor in its protonated form as obtained using DFT/B3LYP/6-311G(d,p) method.*

3.7.4. Proposed Mechanism of Inhibition

The literature shows that most organic molecules develop their resistance to inhibit the corrosion process by adsorption on the metal substrate in a corrosive environment. [15], In our recent research, we use all experimental and theoretical results in order to propose an adsorption mechanism of PIMP on the C38 steel surface in the 1 M HCl medium (Scheme 3). The DFT theoretical approach shows that there is only one protonation which happens at the nitrogen atom. This site can be positively charged in 1 M HCl in the "ammonium" form

(PIMPH+). This charged atom can interact with the chloride anions adsorbed on the mild steel surface by the phenomenon of electrostatic nature (physisorption). In addition, the thermodynamic parameters allowed us to say that the two aromatic rings can stabilize this electrostatic effect through chemisorption of the electrons of the benzene ring. [15, 68] The chemical adsorption that produces by coordination bonds, it originates directly from the donor–acceptor interactions between the nucleophilic sites of the compound (such as the free electron pair of the oxygen atom and the electrons of double bonds), and the vacant d-orbitals of the iron. [69] Finally, the electrons of the iron's d-orbital can be passed to the vacant π*-orbit (antiliant) of the Schiff base studied (Back-donation). [15, 69].

Based on this treatment, the adsorption process of the investigated molecule on the surface of the C38 steel can be represented by the following Scheme 3:

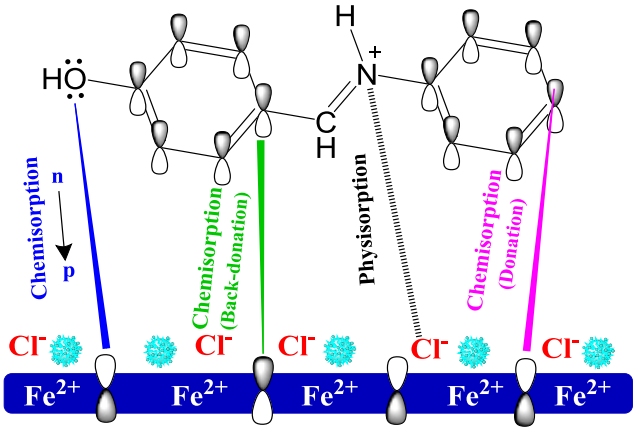

Scheme 3. *Adsorption process of the investigated molecules on the C38 steel surface.*

4. Conclusions

From the results obtained in this study, dealing with PIMP effect on C38 steel corrosion in 1 M HCl medium, several conclusions can be drawn:

Characterization techniques (FTIR, MS, 1H NMR,…) confirm that PIMP was successfully synthetized,

EIS measurement results highlight the improvement of the inhibitive efficiency with increasing PIMP concentration, which reaches its maximum value of 88.1% at 10 mM. We note that 7.5 mM is considered as the optimal concentration,

Potentiondynamic polarization demonstrates that this compound acts as mixed-type inhibitor,

The adsorption of this compound follows the Langmuir adsorption isotherm,

FESEM/EDX observations have confirmed the inhibitor adsorption process and reduction in the surface damage of C38 steel due to corrosion. PIMP prevents C38 steel corrosion by the formation of a very protective film,

Regarding the effect of temperature, we note that the inhibitory efficacy of PIMP inhibitors varies with temperature, confirming desorption of PIMP from the C38 steel surface. We note that 30 ℃ is considered as the optimal temperature.

The local reactivity and distribution of the electronic density of HOMO/LUMO shows that the molecules analyzed contain highly reactive centers distributed throughout the molecular structure which are the cause of their inhibitory properties. Protonated form of PIMP has a better inhibition efficiency than its neutral form.

Abbreviations

PIMP: 4-((phenylimino)methyl) Phenol
OCP: Open Circuit Potential
EIS: Electrochemical Impedance Spectroscopy
PDP: PotentioDynamic Polarization
FESEM: Field Emission Scanning Electron Microscopy
EDX: Energy Dispersive X-Ray
DFT: Density Functional Theory
FTIR: Fourier Transform Infrared Spectroscopy
MS: Mass Spectroscopy
^{1}H NMR: Proton Nuclear Magnetic Resonance
PTFE: PolyteTraFluoroEthylene
FRA: Frequency Response Analyzer
GPES: General Purpose Electrochemical Software
LSV: Linear Sweep Voltammetry
FMO: Frontier Molecular Orbitals
MAC: Mulliken Atomic Charge
HOMO: Highest Occupied Molecular Orbitals
LUMO: Lowest Unoccupied Molecular Orbitals
MEP: Mapped Electrostatic Potential

Supplementary Material

The supplementary material can be accessed at https://doi.org/10.11648/j.mc.20241201.12

Author Contributions

Armel Megha Nouteza: Conceptualization, Resources, Formal Analysis, Writing - original draft, Methodology

Martin Pengou: Conceptualization, Formal Analysis, Data curation, Supervision, Validation, Investigation, Writing - original draft, Methodology, Visualization, Project administration, Writing - review & editing

Joliot Perrin Mbiamy Ngamy: Resources, Methodology

Pengkun Hou: Conceptualization, Investigation, Writing - original draft

Jean Jacques Kouadjo Tchekwagep: Conceptualization, Writing - original draft, Methodology

Charles Péguy Nanseu-Njiki: Conceptualization, Supervision, Investigation, Writing - original draft, Methodology, Writing - review & editing

Emmanuel Ngameni: Conceptualization, Software, Formal Analysis, Supervision, Validation, Investigation, Methodology, Visualization, Writing - review & editing

Conflicts of Interest

The authors declare no conflicts of interest.

References

[1] Faustin, M., Maciuk, A., Salvin, P., Roos, C., Lebrini, M. Corrosion inhibition of C38 steel by alkaloids extract of Geissospermum laeve in 1M hydrochloric acid: Electrochemical and phytochemical studies. *Corrosion Science.* 2015, 92, 287-297.

[2] Rikkouh, R., Douati, T., Hamani, H., Al-Noaimi, M., Chafaa, S. Inhibition effect of 4, 4′-thio bis {N-[(E)-phenol-3-ylmethylidene] aniline} on the corrosion of mild steel in HCl solution under stagnant condition and hydrodynamic flow. *Journal of Adhesion Science and Technology*, 2020, 34(13), 1-26. https://doi.org/10.1080/01694243.2019.1708671

[3] Boucherit, L., Al-Noami, M., Daoud, D., Douadi, T., Chafai, N., Chafaa, S. Synthesis, characterization and the inhibition activity of 3-(4-cyanophenylazo)-2, 4-pentanedione (L) on the corrosion of carbon steel, synergistic effect with other halide ions in 0.5 M H_2SO_4. *Journal of Molecular Struture*, 2019, 1177, 371-380.

[4] M. Barbalat. Apport des techniques électrochimiques pour l'amélioration de l'estimation de l'efficacité de la protection cathodique des canalisations enterrées. Thèse de doctorat, Université de La Rochelle, France, 2012.

[5] M. Messali, M. Larouj, H. Lgaz, N. Rezki, F. Al-Blewi, and M. Chung, "A new schiff base derivative as an effective corrosion inhibitor for mild steel in acidic media: Experimental and computer simulations studies." *Journal of Molecular Structure*, 2018, 1168, 39-48.

[6] M. Gurudatt, N. Mohana, "Synthesis of new pyridine based 1, 3, 4-oxadiazole derivatives and their corrosion inhibition performance on mild steel in 0.5 M hydrochloric acid." *Industrial Engineering Chemistry Research*, 2014, 53(6), 2092-2105. https://doi.org/10.1021/ie402042d

[7] R. Hsissou, S. Echihi, B. Benzidia, S. Cherrouf, R. Haldhar, P. Ahmad, S. Kaya, G. Serdaro and A. Zarrouk, "Performance of curing epoxy resin as potential anticorrosive coating for carbon steel in 3.5% NaCl medium: Combining experimental and computational approaches" *Chemical Physics Letters*, 2021, 783(139081).

[8] M. El-Raouf, E. Khamis, T. Kana, and N. Negm, "Electrochemical and quantum chemical evaluation of new bis (coumarins) derivatives as corrosion inhibitors for carbon steel corrosion in 0.5 M H_2SO_4." *Journal of Molecular Liquid*, 2018, 255, 341-353.

[9] A. Zeino, I. Abdulazeez, M. Khaled, M. Jawich and I. Obot, "Mechanistic study of polyaspartic acid (PASP) as eco-friendly corrosion inhibitor on mild steel in 3% NaCl aerated solution." *Journal of Molecular Liquids*, 2018, 250, 50-62.

[10] A. Ifzan, S. Aamer, A. Pervaiz, A. Syeda, and N. Muhammad, "Bis-Schiff bases of 2,20-dibromobenzidine as efficient corrosion inhibitors for mild steel in acidic medium."*Royal Society of Chemistry*, 2020, 10, 4499–4511. https://doi.org/10.1039/C9RA06443E

[11] A. Ameri, G. Khodarahmi, H. Forootanfar, F. Hassanzadeh and G. Hakimelahi, "Hybrid Pharmacophore Design, Molecular Docking, Synthesis, and Biological Evaluation of Novel Aldimine-Type Schiff Base Derivatives as Tubulin Polymerization Inhibitor." *Chemistry and Biodiversity*, 2018, 15(3), 1612-1872. https://doi.org/10.1002/cbdv.201700518

[12] L. Matos, M. Taborda, E. D'Elia and P. Rodrigues. "Application of an Acid Extract of Barley Agro-Industrial Waste as a Corrosion Inhibitor for Stainless Steel AISI 304 in H_2SO_4." *International Journal of Electrochemical Science*, 2018, 13, 1577-1593.

[13] S. Sangeeta, K. Ahmad, N. Noorussabah and M. Choudhary, "Synthesis, crystal structures, molecular docking and urease inhibition studies of Ni (II) and Cu (II) Schiff base complexes." *Journal of Molecular Structure*, 2018, 1156, 1-11.

[14] M. Hany, A. El-Lateef, A. Kamal and H. Ahmed, "Novel synthesized Schiff Base-based cationic gemini surfactants: Electrochemical investigation, theoretical modeling and applicability as biodegradable inhibitors for mild steel against acidic corrosion." *Journal of Molecular Liquids*, 2017, 232, 478-498.

[15] F. Benhiba, R. Hsissou, Z. Benzekri, S. Echihi, J. El-Blilak, S. Boukhris, A. Bellaouchou, A. Guenbour, H. Oudda, I. Warad, N.K. Sebbar, and A. Zarrouk, "DFT/electronic scale, MD simulation and evaluation of 6-methyl-2-(p-tolyl)-1,4-dihydroquinoxaline as a potential corrosion inhibition." *Journal of Molecular Liquids*, 2021 335(116539).

[16] O. R. Wamba-Tchio, M. Pengou, A-L. Teillout, C. Baumier, I. M. Mbomekallé, P. De Oliveira, C. P. Nanseu-Njiki, and E. Ngameni, "Electrochemical study and experimental simulation of the synergistic effect of a formulation based on Ficus pumila Linn. Leaves extract and zinc sulfate on the XC38 steel corrosion inhibition in NaCl solution." *Journal of Electroanalytical Chemistry*, 2022, 919(116553).

[17] F. Tezcan, G. Yerlikaya, A. Mahmood and G. Kardas, "A novel thiophene Schiff base as an efficient corrosion inhibitor for mild steel in 1.0M HCl: Electrochemical and quantum chemical studies." *Journal of Molecular Liquid*, 2018, 269 398–406.

[18] S. Prakash, "Schiff bases: An overview of their corrosion inhibition activity in acid media against mild steel." *Chemical Engineering Communication*, 2019, 207(7). https://doi.org/10.1080/00986445.2019.1630387

[19] E. Yousif, K. Al-Sammarrae, N. Salih, J. Salimon, and B. Abdullah, "Metal complexes of Schiff base: Preparation, characterization and antibacterial activity." *Arabian Journal of Chemistry*, 2017, 10, 1639-1644.

[20] W. Al-Zoubi, "Biological Activities of Schiff Bases and Their Complexes: A Review of Recent Works." *Interrnational Journal of Organic Chemistry*, 2013, 3, 73-95. https://doi.org/10.4236/ijoc.2013.33A008

[21] A. Abu-Dief, and I. M. A. Mohamed, "A review on versatile applications of transition metal complexes incorporating Schiff bases." *Ben-Suef University Journal of Basic Applied Science*, 2015, 4, 119-133.

[22] R. N. Bader, "Applications of Schiff's bases chelates in quantitative analysis: A review." *Rasayan Journal of Chemestry*, 2010, 3, 660-670.

[23] A. M. Hegazy, "A novel Schiff base-based cationic gemini surfactants: Synthesis and effect on corrosion inhibition of carbon steel in hydrochloric acid solution." *Corrosion Science*, 2009, 51, 2610–2618.

[24] A. N. Nabel and F. Z. Mohamed, "Corrosion inhibition efficiency of nonionic Schiff base amphiphiles of p-aminobenzoic acid for aluminum in 4N HCL." *Colloids and Surface A: Physicochemical and Engineering Aspects*, 2008, 322, 97-102.

[25] S. M. A. Hosseini, and A. Azimi, "The inhibition effect of the new Schiff base, namely 2,20 -[bis-N(4-choloro benzaldimin)]-1,10-dithio against mild steel corrosion." *Materials and Corrosion*, 2008, 59, 41-45. https://doi.org/10.1002/maco.200704101

[26] A. Bala, G. Vikas, S. Kumar and H. Om, "Experimental Investigation of Isatin Schiff base as Corrosion Inhibitor for Carbon Steel in 1M HCl." *International Journal of Scientific Research in science, Engineering and Technology*, 2018, 4(1), 744-754.

[27] S. K. Saha and P. Banerjee, "Introduction of newly synthesized Schiff base molecules as efficient corrosion inhibitors for mild steel in 1 M HCl medium: an experimental, density functional theory and molecular dynamics simulation study." *Materials Chemistry Frontiers*, 2018, 2, 1674-1691. https://doi.org/10.1039/C8QM00162F

[28] L. Boucherit, T. Douadi, N. Chafai, M. Al-Noaimi and S. Chafaa, "The inhibition Activity of 1, 10-bis (2-formylphenyl)-1, 4, 7, 10-tetraoxadecane (Ald) and its Schiff base (L) on the Corrosion of Carbon Steel in HCl: Experimental and Theoretical Studies." *International Journal of Electrochemistry Science*, 2018, 13, 3997-4025.

[29] K. R. Ansari, M. A. Quraishi, and S. Ambrish, "Schiff's base of pyridyl substituted triazoles as new and effective corrosion inhibitors for mild steel in hydrochloric acid solution." *Corrosion Science*, 2014, 79, 5-15.

[30] M. Behpour, N. Mohammadi, N. Soltani, and M. Salavati-Niasari, "Investigation of some Schiff base compounds containing disulfide bond as HCl corrosion inhibitors for mild steel." *Corrosion Science*, 2010, 52, 4046-4057.

[31] A. Dadgarnezhad, F. Baghaei, "Corrosion inhibitory effects of a new synthetic symmetrical Schiff-base on carbon steel in acid media." *Anti-Corrosion Methods and Materials*, 2004, 51, 266-271. https://doi.org/10.1108/00035590410541337

[32] N. A. Negm, I. A. Aiad, M. F. Zaki, and M. Said, "Investigation the inhibitory action of novel diquaternary Schiff dibases on the acid dissolution of carbon steel in 1 M hydrochloric acid solution." *Corrosion Science*, 2012, 65, 77-86.

[33] N. Z. Hashim, K. Kassim, and Y. Mohd, "Corrosion inhibition of mild steel by N-phenyl-1,4-phenylenediamine and its Schiff base derivatives in 1M HCl." *Academy of Management Review*, 2012, 554, 408-413. https://doi.org/10.4028/www.scientific.net/AMR.554-556.408

[34] N. A. Jonnie, O. O. Lukman, S. A. Abolanle, and E. E. Eno, "A novel Schiff base of 3-acetyl-4-hydroxy-6-methyl-(2H) pyran-2-one and 2,2'-(ethylene-dioxy)diethylamine as potential corrosion inhibitor for mild steel in acidic medium." *Materials and Corrosion*, 2015, 8, 2918-2934. https://doi.org/10.3390/ma8062918

[35] C. Kustu, and O. Atakol, "Schiff bases of increasing complexity as mild steel corrosion inhibitors in 2 M HCl." *Corrosion Science*, 2007, 49, 2800-2814.

[36] O. R. Wamba-Tchio, M. Pengou, A-L. Teillout, C. Baumier, I. M. Mbomekallé, P. De Oliveira, C. P. Nanseu-Njiki, and E. Ngameni, "Comparison between Lacunary and Saturated Keggin Polyoxometalates as Steel Corrosion Inhibitors in Chloride Solution: Contribution of the Lacuna in the Inhibition Mechanism." *Chemistry Select*, 2020, 32(5), 10135-10143. https://doi.org/10.1002/slct.202001591

[37] W. Zhang and Y. C. Wu, "Gravimetric, electrochemical and surface studies on the anticorrosive properties of 1-(2-pyridyl)-2-thiourea and 2-(imidazol-2-yl)-pyridine for mild steel in hydrochloric acid." *New Journal of Chemistry*, 2018, 42(15), 12649–12665. https://doi.org/10.1039/C8NJ01762J

[38] N. Soltani, N. Tavakkoli, and M. Khayatkashani, "Green approach to corrosion inhibition of 304 stainless steel in hydrochloric acid solution by the extract of Salvia officinalis leaves." *Corrosion Science*, 2012, 62, 122–135.

[39] U. Eduok, O. Faye, and J. Szpunar, "Corrosion inhibition of X70 sheets by a film-forming imidazole derivative at acidic pH." *Royal Society of Chemistry Advans*, 2016, 6, 108777–108790. https://doi.org/10.1039/C6RA23099G

[40] M. Faustin, "Étude de l'effet des alcaloïdes sur la corrosoion de l'acier C38 en milieu acide chlorhydrique 1M: application à Aspidosperma album et Geissospermum laeve (Apocynacées)." Thèse de Doctorat, Université Antilles-Guyane, France, 2013.

[41] M. Yadav, S. Kumar, N. Tiwari, I. Bahadur, and E. E. Ebenso, "Experimental and quantum chemiccal studies of synthesized triazine derivatives as an efficient corrosion inhibitor for N80 steel in acidic medium." *Journal of Molecular Liquid*, 2015, 212, 151-167.

[42] B. Khalissa, M. Ouahiba, and H. Abdelkader, "Synthesis, spectroscopic characterization and a comparative study of the corrosion inhibitive efficiency of an a-aminophosphonate and Schiff base derivatives: Experimental and theoretical investigations." *Journal of Molecular Structure*, 2018, 1157, 165-176.

[43] S. S. A. Mohamed, M. Hany, and A. Kamal, "Anionic oxide'vanadium Schiff base amino acid complexes as potent inhibitors and as effective catalysts for sulfides oxidation: Experimental studies complemented with quantum chemical calculations." *Journal of Molecular Liquid*, 2018, 250, 307-322.

[44] K. R. Ansari, M. A. Quraishi, M. A. J. Mazumder, and S. Ambrish, "Chitosan Schiff base: an environmentally benign biological macromolecule as a new corrosion inhibitor for oil & gas industries." *International Journal of Biological Macromolecules*, 2019, 144, 305-315.

[45] S. Sanjoy, K. S. Sourav, and S. Dipankear, "Adsorption and anti-corrosion characteristics of vanillin Schiff bases on mild steel in 1 M HCl: experimental and theoretical study." *Royal Society of Chemical Advans*, 2020, 10, 9258–9273. https://doi.org/10.1039/C9RA07982C

[46] B. Imene, D. Tahar, and C. Salah, "Heterocyclic Schiff bases as corrosion inhibitors for carbon steel in 1 M HCl solution: hydrodynamic and synergetic effect. *Journal of Dispersion Science and Technology*, 2019, 41(7), 1002-1021. https://doi.org/10.1080/01932691.2019.1614038

[47] P. Kumari, P. Shetty, and S. A. Rao, "Electrochemical Measurements for the Corrosion Inhibition of Mild Steel in 1M Hydrochloric Acid by Using an Aromatic Hydrazide Derivative." *Arabic Journal of Chemistry*, 2017, 5, 653–663.

[48] M. Lebrini, M. Lagren ée, and F. Bentis, "Electrochemical and Quantum Chemical Studies of New Thiadiazole Derivatives Adsorption on Mild Steel in Normal Hydrochloric Acid Medium." *Corrosion Science*, 2015, 47, 485-505.

[49] N. D. Gowraraju, E. E. Ebenso, and S, Chitra, "Adsorption Characteristics of Iota-Carrageenan and Inulin Biopolymers as Potential Corrosion Inhibitors at Mild Steel/Sulphuric Acid Interface." *Journal of Molecular Liquid*, 2017, 232, 9-19.

[50] F. A. Azeez, O. A. Al-Rashed, and A. A. Nazeer, "Controlling of Mild-Steel Corrosion in Acidic Solution Using Environmentally Friendly Ionic Liquid Inhibitors: Effect of Alkyl Chain." *Journal of Molecular Liquid*, 2018, 265, 654-663.

[51] H. Ashassi-Sorkhabi, B. Shaabani, and D. Seifzadeh, "Corrosion inhibition of mild steel by some schiff base compounds in hydrochloric acid." *Applied Surface Science*, 2005, 239, 154-164.

[52] Y. A. Ongun, M. B. Dogru, G. Kardas, and B. Yazıcı, "Electrochemical and quantum chemical studies of 2-amino-4-methyl-thiazole as corrosion inhibitor for mild steel in HCl solution." *Corrosion Science*, 2014, 83, 310-316. https://doi.org/10.1016/j.corsci.2014.02.029

[53] S. Kumar, P. Yadav, and M. Yadav, "Experimental and quantum chemical studies on corrosion inhibition effect of synthesized organic compounds on N80 steel in hydrochloric acid." *Indian Engineering Chemical Research*, 2013, 52(39), 14019-14029. https://doi.org/10.1021/ie401308v

[54] M. A. Hegazy, A. H. Bedair, and M. A. Sadeq, "An investigation of three novel nonionic surfactants as corrosion inhibitor for carbon steel in 0.5 M H_2SO_4." *Corrosion Science*, 2012, 54, 219-230.

[55] A. Kokalj, "Corrosion inhibitors: physisorbed or chemisorbed?" *Corrosion Science*, 2022, 196(109939).

[56] B. Ngoune, M. Pengou, A. N. Megha, C. P. Nanseu-Njiki, and E. Ngameni, "Performances of Alkaloid Extract from Rauvolfia macrophylla Stapf toward Corrosion Inhibition of C38 Steel in Acidic Media." *ACS OMEGA*, 2019, 4, 9081−9091. https://doi.org/10.1021/acsomega.9b01076

[57] B. Ngoune, M. Pengou, C. P. Nanseu-Njiki, and E. Ngameni, "A comparative study using solution analysis, electrochemistry and mass change for the inhibition of carbon steel by the plant alkaloid Voacangine." *Corrosion Engineering Science and Technology*, 2020, 55(2), 138-144. https://doi.org/10.1080/1478422X.2019.1700654

[58] A-A. Ahmed, S. Lina and S. T. Mohd, "Quantum chemical elucidation on corrosion inhibition efficiency of Schiff base: DFT investigations supported by weight loss and SEM techniques." *International Journal of Low-Carbon Technology*, 2019, 00, 1-8. https://doi.org/10.1093/ijlct/ctz074

[59] K. Fukui, T. Yonezawa, C. Nagata, and H. Shingu, "Molecular orbital theory of orientation in aromatic, heteroaromatic, and other conjugated molecules." *Journal of Chemical Physics*, 1954, 22(8), 1433–1442. https://doi.org/10.1063/1.1740412

[60] L. Guo, S. Zhu, S. Zhang, Q. He, and W. Li, "Theoretical studies of three triazole derivatives as corrosion inhibitors for mild steel in acidic medium." *Corrosion Science*, 2014, 87, 366-375.

[61] A. Y. Musa, A. Kadhum, A. Mohamad, A. Rahoma, and H. Mesmari, "Electrochemical and Quantum Chemical Calculations on 4,4-Dimethyloxazolidine-2-Thione as Inhibitor for Mild Steel Corrosion in Hydrochloric Acid." *Journal of Molecular Structure*, 2010, 969, 233-237.

[62] M. Mahdavian, S. Farashi, S. Javadian and F. Ektefa, "Corrosion of Mild Steel in Hydrochloric Acid Solution in the Presence of Two Cationic Gemini Surfactants with and without Hydroxyl Substituted Spacers." *Corrosion Science*, 2018, 137, 62-75.

[63] H. Ju, Z. P. Kai, and Y. Li, "Aminic nitrogen-bearing polydentate Schiff base compounds as corrosion inhibitors for iron in acidic media: a quantum chemical calculation." *Corrosion Science*, 2008, 50, 865-871.

[64] I. B. Obot, D. D. MacDonald, and Z. M. Gasem, "Density functional theory (DFT) as a powerful tool for designing new organic corrosion inhibitors. Part 1: an overview." *Corrosion Science*, 2015, 99, 1-30.

[65] A. Kokalj, S. Peljhan, M. Finsgar, and I. Milosev, "What determines the inhibition effectiveness of ATA, BTAH, and BTAOH corrosion inhibitors on copper?" *Journal of Amer-iccan Chemial Society*, 2010, 132, 16657-16668. https://doi.org/10.1021/ja107704y

[66] S. Q. Hu, A. L. Guo, Y. G. Yan, X. L. Jia, Y. F. Geng, and W. Y. Guo, "Computer simulation of diffusion of corrosive particle in corrosion inhibitor membrane." *Computational and Theoretical Chemistry*, 2011, 964, 176-181.

[67] R. Hsissou, F. Bentis, M. El-Aboubi, S. Abbout, Z. Benzekri, Z. Safi, M. Rafik, H. Bahaj, M. Kaba, M. Galai, N. Wazzan, S. Briche, S. Boukhris, A. Zarrouk, M. EbnTouhami, and M. Rafik, "Synthesis and performance of two ecofriendly epoxy resins as a highly efficient corrosion inhibition for carbon steel in 1 M HCl solution: DFT, RDF, FFV and MD approaches." *Chemical Physics Letters*, 2022, 806(139995).

[68] N. Chaubey, V. K. Singh, and M. A. Quraishi, "Papaya peel extract as potential corrosion inhibitor for Aluminium alloy in 1M HCl: Electrochemical and quantum chemical study." *Ain Shams Engineering Journal*, 2018, 8(4), 1131-1140.

[69] Singh, P., Quraishi, M. A. "Corrosion inhibition of mild steel using Novel Bis Schiff's Bases as corrosion inhibitors: Electrochemical and Surface measurement." ISO4 *Journal of Measurement*, 2016, 86, 114-124.